# Beyond Evanescent Electromagnetic Fields: Via Metal Wireless Surface Wave Power - Data transmission System and Wireless Power Transfer Based Sensor

## Sai Kiran Oruganti

A thesis submitted in partial fulfillment for the

degree of Doctor of Philosophy

ELECTRICAL ENGINEERING



School of Electrical and Computer Engineering

Ulsan National Institute of Science and Technology

Republic of Korea

**ULSAN NATIONAL INSTITUTE OF SCIENCE AND TECHNOLOGY**

**Beyond Evanescent Electromagnetic Fields: Via Metal Wireless Surface Wave Power - Data transmission System and Wireless Power Transfer Based Sensor**

by

Sai Kiran Oruganti

A thesis submitted in partial fulfillment for the

degree of Doctor of Philosophy

in the

ELECTRICAL ENGINEERING

School of Electrical and Computer Engineering

January 2016

# Declaration of Authorship

I, SAI KIRAN ORUGANTI, declare that this thesis titled, '' and the work presented in it are my own. I confirm that:

- This work was done wholly or mainly while in candidature for a PhD Degree at this Ulsan National Institute of Science and Technology, Ulsan.

- Where any part of this thesis has previously been submitted for a degree or any other qualification at this University or any other institution, this has been clearly stated.

- Where I have consulted the published work of others, this is always clearly attributed.

- Where I have quoted from the work of others, the source is always given. With the exception of such quotations, this thesis is entirely my own work.

- I have acknowledged all main sources of help.

- Where the thesis is based on work done by myself jointly with others, I have made clear exactly what was done by others and what I have contributed myself.
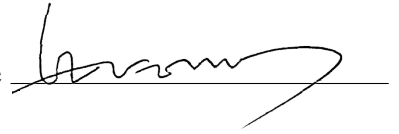

Signed:

_____


Date:

_____

**Prof. Dr. Franklin Bien⁺**     Adviser     Signature _____

**Prof. Dr. Jingook Kim⁺**     Committee Member     Signature _____

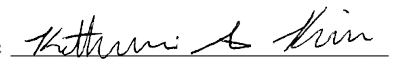**Prof. Dr. Ki Jin Han⁺**     Committee Member     Signature _____

**Prof. Dr. Katherine Kim⁺**     Committee Member     Signature _____

**Prof. Dr. Sung Tae Hong#**     Committee Member     Signature _____

Date: ____02.12.2015____     Place:____Ulsan____

+    School of Electrical Engineering    Ulsan National Institute of Science and Technology

#    School of Mechanical Engineering    Ulsan National Institute of Science and Technology

# Abstract

The presented thesis explores the evanescent electromagnetic waves concept to design wireless transmission to address two difficult practical engineering problems (a.)Wireless power/data transmission across metal complexes such as ships, submarines, oil-rigs is a challenging engineering problem. Primarily, due to the fact that the wireless electromagnetic waves undergo electromagnetic interference shielding due to the metal structures. Henceforth marine vessels utilize wired systems. An average ships requires several kilo-meters of cables just to establish communications. Apart from this, critical systems such as safety alarms require continuous power supply. Unfortunately, the back up fault detection systems of the fire alarms rely on cables. In an event of cable snapping fault detection systems fail. These factors become even more serious in case of oil-rigs and submarines. The solution presented in this thesis establishes noise free wireless radio communication across several metal floors (300 meters)and continuous wireless power supply of 16watts and 40 watts upto 4 meters and 1.2 meters, respectively. This is done by utilizing the concept of establish surface electromagnetic waves over metal air interfaces, which travel in a backward and forward fashion on the metal surfaces. (b.) An all in one touch, proximity and hover sensor system, whose performance does not degrade as the size of the touch screen panels increase or are contoured. The degraded performance stems from the large RC-time constant delays. This thesis addresses this problem by using a wireless power transfer based sensor system. Wireless power transfer systems transmit power at optimal efficiency under resonance matched conditions, the human body offers bio-electrical impedance. Hence, an approaching human finger shall disturb the resonance, which causes a drop in efficiency. This drop in efficiency can be registered as touch, proximity or hover sensing. Being wireless it has longer range and linearity as compared to capacitive sensors, resistive sensors or inductive sensors. The sensor presented in this thesis is based on evanescent wireless power transmission, implying that the electromagnetic waves decay exponentially normal to the surface of the transmitter. This property of the system has advantages as it does not effect the nearby electronic circuitry. The sensor performs normal even when placed under LCD screen under ON condition. Also, there is no performance degradation observed in the electronic system such as the LCD screen.

# Acknowledgements

# Contents

# List of Figures

# List of Tables

# Physical Constants

| | | | |
|---|---|---|---|
| Speed of Light | $c$ | $=$ | $2.997\,924\,58 \times 10^8$ ms$^{-\text{S}}$ (exact) |
| Free space permittivity | $\epsilon_0$ | $=$ | $8.854187817 \times 10^{-12} F/m$ |
| Free space permeability | $\mu$ | $=$ | $1.25663706 \times 10^{-6} m.kg.s^{-2}.A^{-2}$ |

# Symbols

| | | |
|---|---|---|
| $A$ | Period of the periodic surface | |
| $\Gamma$ | Vector field Component | |
| $f_n$ | transverse dependence of n-th space harmonic vector field component | |
| $b_0$ | Fundamental propagation constant | |
| $E_z^{inc}$ | Incident $z$-component of $E$-field | |
| $E_z^{Scat}$ | Scattered $z$-component of $E$-field | |
| $\phi^{inc}$ | Incident angle | |
| $\phi^{Scat}$ | Scattered angle | |
| $\lambda_0$ | Wavelength | |
| $\epsilon_r$ | Relative permittivity | |
| $f_{Resonance}$ | Resonance frequency | $Hz$ |
| $L$ | Inductance | $Henry, H$ |
| $R$ | Resistance, | $Ohm, \Omega$ |
| $C$ | Capacitance | $Farad, F$ |
| $P$ | power | W (Js$^{-1}$) |
| $P_{Dissipation}$ | Dissipated power | |
| $H$ | Magnetic field component | |
| $X_s$ | Surface reactance | $\Omega$ |
| $W_e^{evanescent}$ | Evanescent Energy | |
| $t_{coppercoil}$ | thickness copper coil of the cylindrical coil | $m$ |
| $Area$ | Area of the cavity receiver | $m^2$ |

| | | |
|---|---|---|
| $C_{metal-Rx}$ | Capacitance between metal and receiver | F |
| $C_{metal-Tx}$ | Capacitance between metal and transmitter | F |
| $\eta$ | Efficiency | |
| $X(f)_{ind}$ | inductive reactance of the sheet like waveguide | $\Omega$ |
| $g$ | mesh period | $m$ |
| $\omega$ | angular frequency | $rads^{-1}$ |

*Dedicated to Nikola Tesla, M.Vishveshwarayya,
Vivekananda & A.P.J. Abdul Kalam*

# Chapter 1

# Introduction

## 1.1 Introduction

Consider two interesting real-time problems

- Ships & Oil Rigs, where radio frequency(RF) waves or for that matter , electromagnetic(EM) waves cannot travel through metal complexes to convey information or transmit power wirelessly [1]-[4].

- Large contoured touch screen panels(TSP) witness inferior performance in terms of speed. Primarily due to large RC-time constant delays incurred, which are caused by the increased resistance and capacitance parameters as the size of the TSP's increase [5]-[7].

Now lets consider each of these two real-time problems in a bit of details.

### 1.1.1 Communication and Power Transfer in Ships and Oil Rigs

A well known problem in the shipping and oil rig industry is the electromagnetic interference (EMI) shielding of the EM waves offered by the metal complexes[2]. For this reason, both these industries deploy cables to convey data or communication signals.

**Limitations due to cables.**

A cabled solution is although straight forward, but it is not preferable for several reasons

- *Structural integrity.* Often holes are needed to be drilled to install cables, this compromises with the structural integrity of the ship or oil-rigs[1],[2].

- *Cable Failure.* The cable snapping and short circuit, resulting to fire accident is an ever present danger.

- *Length.* An average ship requires several kilometers of cable length.

- *Installation effort,time and maintenance.* Installation requires not only drilling holes, but to also provide the cables with proper supporting brackets.

- *High Voltage levels.* Nominal voltage levels to sustain reliable communications is 250 V. Which is very high for human crew to work with an close proximity, given the ship or rig is a giant metal structure.

- *Non-ionizing radiation.* Is an ever present invisible threat to the crew.

- *Mobility.* Finally, wired communication systems restrict the mobility of the crew on board.

## 1.1.2 Room for wireless EM transmission

Even though through air radio transmission is shielded down, the marin vessels are not exactly perfectly enclosed structures. There is enough room created by ventilation ducts neoprene gaskets of the watertight doors, as shown in fig1.1.

Consider fig. 1.2 , which depicts the through metal wall penetration free wireless power/data transfer system based on Piezoelectric Ultrasonic Transducer(PUT) and Electro Magnetic Acoustic Transducer(EMAT) transceivers to transmit power/data across two metal walled rooms. The transceivers need to be coaxially aligned in order for any transmission of data and power from point A to point B [1], [2]. However, in order to transmit signal from point A to point D, both PUT and EMAT would require additional
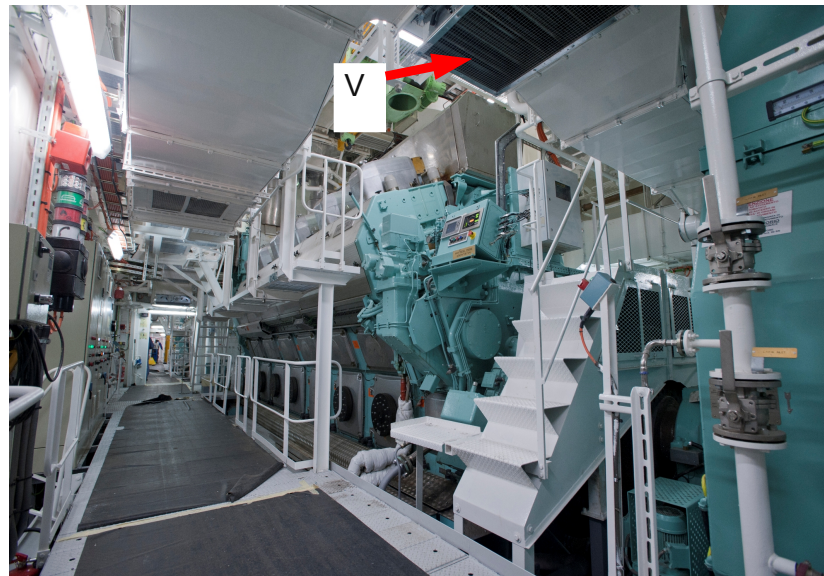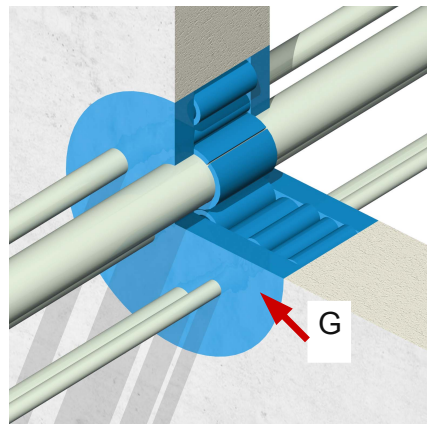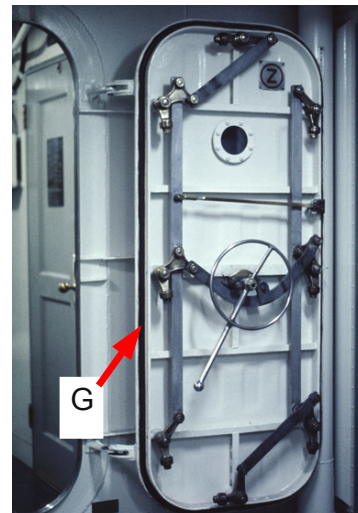
FIGURE 1.1: Spaces within a ship (a) Ventilator, represented by V, (b) Pipe wall transit system, gasket G, (c) Water tight door neoprene gasket, G .

electronic components or modules. Which include four signal amplifiers and two wireless devices to transmit through air. For a practical realization this poses problems with respect to maintenance and cost.
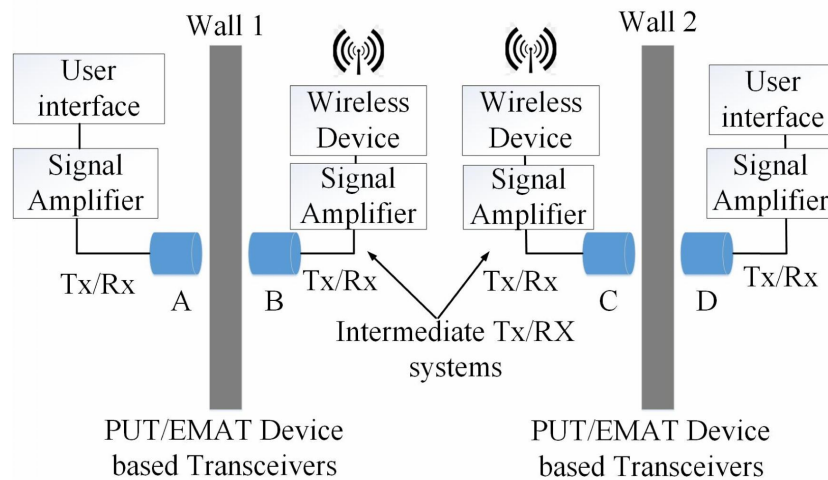
FIGURE 1.2: Existing Methods: PUT and EMAT.

### 1.1.3 Large Contoured Touch Screen Panel RC Time Constant Delays

With the increasing size of the the TSP, the RC time constant delay increases. At the same time the timing delay issues for large contoured display screens arise due to the change in the sheet resistance of the displays when they are curved[8]. Following are the issues with the existing touch, proximity and hover sensing solutions:

- *Conductivity of Target Object.* Although capacitive touch sensor is fast, but the sensitivity and range depends on conductivity of target object[5].

- *Linearity.* resistive type touch sensor is linear but slow[6]-[7].

- *Linearity vs Range.* capacitive touch sensor becomes non-linear at very low distances from the sense head[7].

- *Cost vs Response time.* Capacitive is fastest but costly[7]-[9]. At the same time response time reduces as the TSP becomes larger or curved[8]. Although inductive type is also fast and cheap, but it requires stylus to operate[9].

- *All in one :Touch, Proximity and Hover.* So far the existing solutions have not addressed an all in one solution.

## 1.2    Thesis Outline

The chapter 1 articulates two practical problems faced by the industry and how the existing methods are at a disadvantage under certain constraints. The merits of the existing systems have been acknowledged.

The chapter 2 of this thesis focuses on the concept of evanescent fields and surface electromagnetic waves at the metal-air interfaces. The focus has been to use the theoretical model given by Gerson and Nadan for surface electromagnetic modes on ferrite slabs. And the experimental verification of the exponential decay of the electric fields normal to the metal surfaces.

A generalized theory of wireless power transfer based sensors, with evanescent field based power transfer mechanism. The theory focuses on the touch, proximity and hover sensing mechanism of the sensor.

The chapter 3 focuses on the factors governing the design parameters of the sheet like waveguides, cylindrical cavity receivers and spiral coil receiver which have been used to generate surface waves in order to transmit signals across metal complexes. The same factors are also useful in designing the wireless energy transfer based sensor.

The chapter 4 focuses on the results and discussions of the experiments. The voice transmission was carried out in a real-time scenario on an oil-rig. A power transmission across 400 cm was carried out. The wireless power transfer sensor operated without effecting the nearby circuitry.

The chapter 5 presents the conclusions of the presented work, and proposes other applications of the presented work.

# Chapter 2

# Theoretical Aspects: Power/Data and Sensing

## 2.1 Theory of Surfacewave Power and Radio Signal Transfer

Floquet's theorem and evanescent modes: Consider fig 2.1, the wave solutions for periodic structures with a period "A" are described by Floquet's theorem. For a given mode at a given frequency, can be deduced using space harmonics, described by the complex
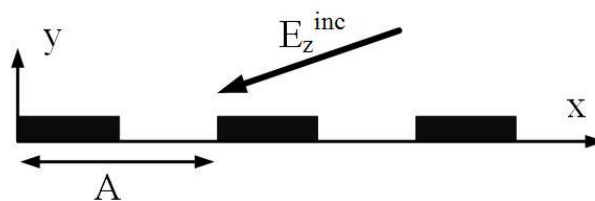


FIGURE 2.1: Incident E-field on a periodic surface.

Fourier series form equation[10]:

$$\Gamma = \sum_{n=-\infty}^{\infty} f_n exp\left(-j\left(b_0 + \frac{2\pi n}{A}\right)z\right) \tag{2.1}$$

Here, $\Gamma$ is the vector field component, and $f_n$ is the transverse dependence of the n-th space harmonic of the vector field component. $b_0$ is the fundamental propagation constant. We are interested in the scattered electric and magnetic field components on the metal surface in this case. The incident and scattered electric field can be given by the following:

$$E_z^{inc}(x,y) = exp\left(jb_0\left(x\cos\phi^{inc} + y\sin\phi^{inc}\right)\right) \tag{2.2}$$

$$E_z^{Scat}(x,y) = \sum_{n=-\infty}^{\infty} c_n(y)exp(jb_{x_n}x) \tag{2.3}$$

Equations 2.2 and 2.3 are the Floquet harmonics functions of the incident and scattered fields, respectively The above two equations must satisfy the following wave equation:

$$\left(\frac{\partial^2}{\partial x^2} + \frac{\partial^2}{\partial y^2} + b_0^2\right)E_z^{Scat} = 0 \tag{2.4}$$

The end result is the determination of the angle of scattering. To maintain the simplicity of the discussion, the derivation has been excluded in this paper. It can be followed up using any standard textbook on this subject. The scattering field in the plane wave expansion format can be written as follows:

$$E_z^{Scat}(x,y) = \sum_{n=-\infty}^{\infty} c_n exp(jb_{x_n})exp(jb_{y_n}|y|)) \tag{2.5}$$

Equation 2.6 describes the scattered field as a component of the forward and backward traveling waves. In addition, a set of multiple propagating modes can be scattered off a given periodic surface. The angles of these modes can be defined by the following equation:

$$b_{x_n} = b_0(\cos\phi^{inc} + \frac{n}{A/\lambda_0}) \tag{2.6}$$

$$b_{y_n} = b_0\sqrt{1 - \left(\cos\phi^{inc} + \frac{n}{A/\lambda_0}\right)^2} \tag{2.7}$$

$$\phi^{scat} = \tan^{-1}\left(\frac{b_{y_n}}{b_{x_n}}\right) \qquad (2.8)$$

Let us visualize the equations by taking a test case, where $\phi^{inc} = 60$ . The period $A = 1.0$ , where the wavelength is given by $\lambda_0$; at n = 0, $\phi^{scat}$ = 60; at n = -1, $\phi^{scat}$ = -60; and at $n = 1$, = 0.0000 +55.1428i (evanescent mode). Now, at $A = 0.5$ , the values are $n(0) = 60$, $n(1) = 0.0000 + 89.7710i$, and $n(-1) = 0.0000$ -55.1428i. We observe two evanescent modes here and one less real angle of scattering compared to the case where $A = 1.0\lambda_0$ . Now, consider a case where $A = 10^{-10}$, i.e., the periodic BCC structure of metal. The values of the scattering angles, other than n = 0, will be infinite. The comparative values have been listed in table 2.1. It is observed that until $10^{-4}\lambda_0$ , no symmetric evanescent modes exist for the angle of scattering. By symmetric, we mean that identical set of negative and positive evanescent modes. At $10^{-4}\lambda_0$ and $10^{-10}\lambda_0$ , a set of symmetric evanescent modes appear. In fact, at $10^{-10}\lambda_0$ , the complex scattering angles have approached infinity. The calculations listed in table 2.1 demonstrate the existence of forward and backward traveling surface waves due to infinite evanescent modes. The positive complex angle values $\phi^{scat}$ are the forward propagating waves, while the negative complex value components are backward propagating waves.

### 2.1.1 Evanescent fields and Floquet's theorem at the metal-air interface

Consider the fig.2.2, where the EM field is being directed into the metal surface. The EM wave undergoes total internal reflection, the grain of steel (body centric cuboid crystal) represented by $G$ and the void or empty space between the first grain and the next grain is depicted by $V$. From the standard chemistry handbook we know that the grain diameter is 90-32 $\mu$m depending on the grain size number 4.0 to 7.0 [11]. While the air molecule diameter is estimated to be roughly $4 \times 10^{-10}m$. Obviously the void size $V = 90 - 32\mu m$, this implies roughly anywhere between 225000 to 80000 air molecules can reside in the void $V$. Although the estimated air molecule diameter is a rough estimation, but it establishes the fact that there exists a metal (grain)-dielectric (air) interface along the metal surface.

TABLE 2.1: Evanescent modes

| $A$ | n | $\phi^{scat}$ |
|---|---|---|
| $1\lambda_0$ | -1 | -60 |
| | 0 | 60 |
| | 1 | 0.0000+55.1428i |
| $2\lambda_0$ | -3 | 0 |
| | -2 | -60 |
| | -1 | -90 |
| | 0 | 60 |
| | 1 | 0 |
| | 2 | 0.0000+55.1428i |
| | 3 | 0.0000 +75.4561i |
| $0.001\lambda_0$ | -1 | 0.0000e+00 - 4.3547e+02i |
| | 0 | 60 |
| | 1 | 0.0000e+00 + 4.3553e+02i |
| $10^{-4}\lambda_0$ | -1 | 0.0000e+00 - 5.6743e+02i |
| | 0 | 60 |
| | 1 | 0.0000e+00+ 5.6743e+02i |
| $10^{-10}\lambda_0$ | -1 | 0.0000-$\infty$ |
| | 0 | 60 |
| | 1 | 0.0000+$\infty$ |
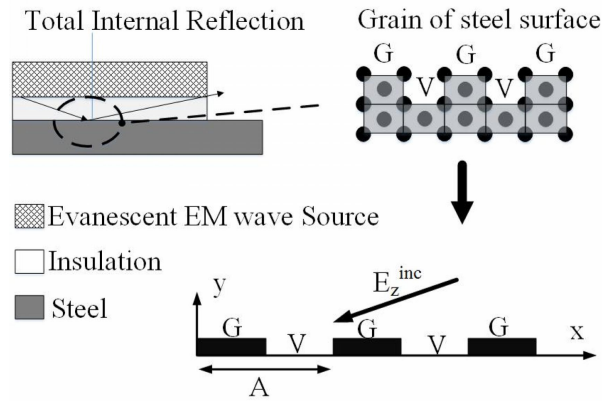


FIGURE 2.2: EM field source directed onto a steel surface undergoes total internal reflection and the inset view of the steel grain $G$ and empty spaces filled by air molecules $V$.

Now, from the theory presented in the previous subsection, the existence of backward and forward surface waves on metal surfaces can easily be visualized.

## 2.2 Existence of Surface Electromagnetic Waves at Metal-Air Interfaces

### 2.2.1 Previous studies

One of the earliest known published works on the surface electromagnetic (SEW) [12], there have been several reported results from the era of erstwhile Soviet Union. A good review on SEW's has been presented in [13]. The SEW's propagate over interfaces of conducting medium and a dielectric medium. [12] - [14].

Zenneck showed that Maxwell's equations with proper boundary conditions give a solution which can be loosely labeled as SEW's. The dispersion relation for SEW's propagating along the interface between media with dielectric permittivities $\epsilon$ and $\epsilon_r$ in the form of [12] :

$$k^2 = k_0^2 \frac{\epsilon_0 \epsilon_r}{\epsilon_0 + \epsilon_r} \tag{2.9}$$

The quantities, $k_0 = \omega/c$ and $\omega$ are the propagation vector and the frequency of the wave. However there have been great deal of criticisms of Sommerfeld's theoretical framework since the beginning of 1919's. There were numerous unsuccessful efforts to excite SEW's under unnatural conditions, as mentioned in the work presented by [14] . However, [14] and [15] have successfully demonstrated the existence of SEW at metal-air interfaces experimentally.

Interestingly, there was one field of physics which saw extensive usage of SEW's, i.e. surface plasmon polaritons (SPP). A generalized definition of SPP is nothing but, light-matter interaction. They are electromagnetic excitations propagating in a longitudinal direction to the metal surfaces, at the juncture of metal-dielectric interfaces. They decay exponentially normal to the surface of the metal [16].

## 2.2.2 Theoretical framework: Surface Electromagnetic Waves in Megahertz Frequency Regime

In 1974, Gerson and Nadan presented a theoretical model of Surface Electromagnetic modes in other words SEW's on the ferrite slabs[17]. Reproducing the theoretical frame work presented by them for the sake of continuity of the discussion. The physical properties of surface waves can be analyzed by applying Maxwell's equations to an interface between a flat metal sheet and air. It is noteworthy that the equations are simply the general form of guiding of EM waves. Beginning with the generalized Maxwell's equations

$$\nabla \times \vec{E} = -\frac{\partial \vec{B}}{\partial t} \tag{2.10}$$

$$\nabla \times \vec{H} = \epsilon \frac{\partial \vec{D}}{\partial t} \tag{2.11}$$

From fig 2.3, and equation 2.11 , the $\epsilon = \epsilon_0$ in the free space region, while it is $\epsilon_0 . \epsilon_m$ in the metal region. The relationship between $B$ and $H$ can be given by:

$$\vec{B} = \mu_0 \vec{H} \tag{2.12}$$

Applying assumptions reported in [17] , that the amplitude of the response of the system under question to the EM excitations is in the range of $\exp(j\omega t)$.

The electric field equations can be represented by:

$$E_z = A.exp[-\beta_a x + j(\omega t - ky)], \qquad x > 0 \tag{2.13}$$

$$E_z = [B \cosh \beta_m x + C \sinh \beta_m x] \exp[j(\omega t - ky)], \quad 0 \geq x \geq -d \tag{2.14}$$

$$E_z = D \exp[\beta_a(x + d) + j(\omega t - ky)], \qquad x < -d \tag{2.15}$$
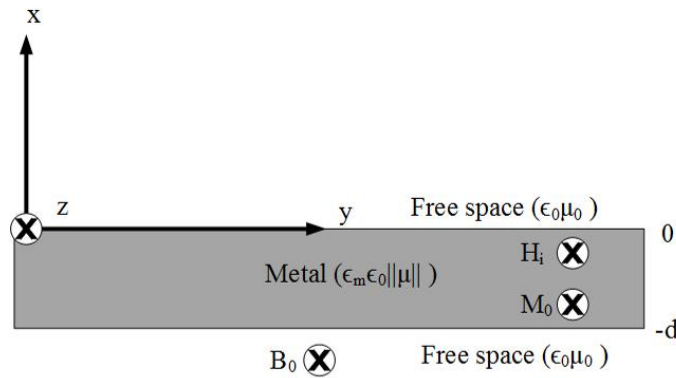
FIGURE 2.3: Field profiles and boundary conditions on metal.

The value of $k$=0.273 (at $13.3MHz$) and $\beta_a$=0.85$k$ extracted as per the approximations reported in [17].

#### 2.2.2.1  Experimental Verification of Gerson and Nadan Model

The existence of SEW's can only be proved by comparing the theoretical model reported in [17] with the experimental results. The experimental setup is shown in fig 2.4.
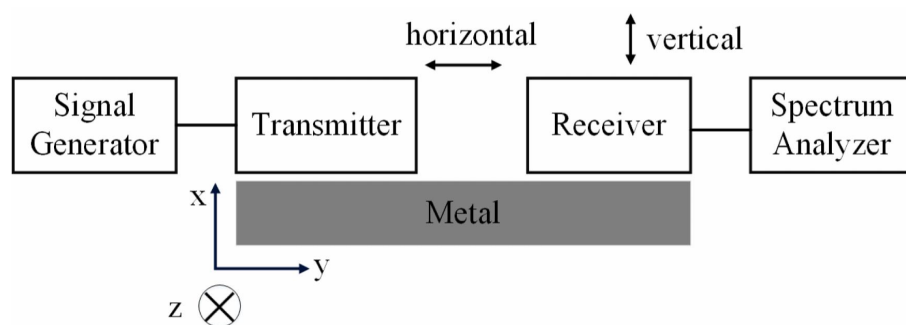


FIGURE 2.4: Experimental setup: spectrum analyzer measurements.
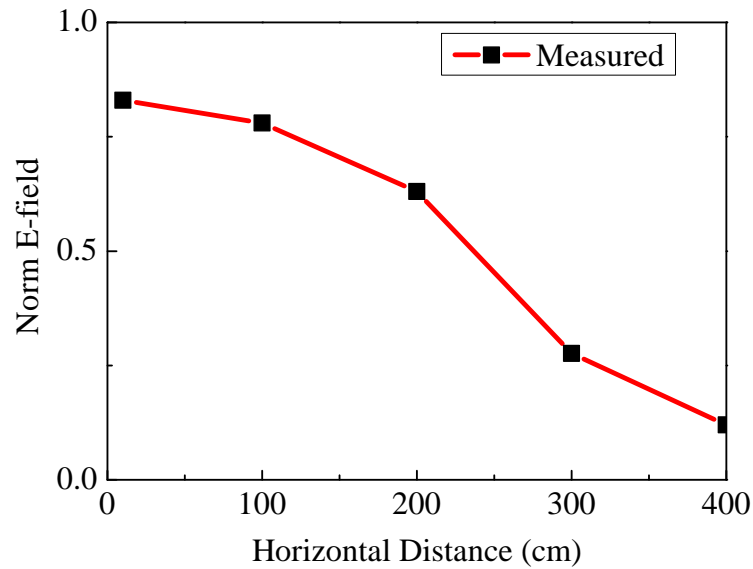
FIGURE 2.5: Measured, received power in horizontal distance.
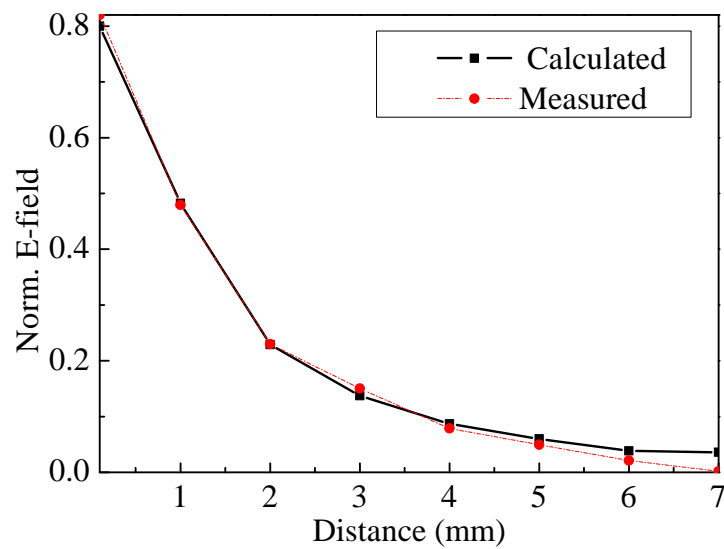


FIGURE 2.6: Calculated and measured, received power: vertical distance of the receiver with respect to the metal.

The signal generator was used as a source to feed a sinusoidal signal of 10 dBm at 13.07 MHz into the transmitter, shooting power into the metal surface and a signal analyzer was used to measure the received power, as shown in fig. 2.4. The reason for

choosing 13.07 MHz can be found in the next section, where the S-parameters have been described. Two set of tests were performed (i.) Horizontal variation of distance between transmitter and receiver from 0 to 400 cm (ii.) Vertical variation of receiver from the metal surface from 0 to 7 mm. The fig 2.5 shows the variation of received power from 0 to 400 cm horizontal distance. The fig.2.6 shows the calculated and measured values of the received power, while receiver distance is varied vertically from 0 to 7 mm.

### 2.2.3   Near-Field Antenna

There exists a number of possible near-field antenna types[15]. However, it is important to design an antenna which can setup a parallel field to the surface of the metal and air interface [17]. For this purpose a sheet like waveguide antenna was chosen, which generates an evanescent field due to the total internal reflection offered to the fed-through EM wave by the conductive ground layer essentially made of copper. When, this antenna is placed in a non-contact form, by sandwiching a non-conductive insulating layer with a finite dielectric constant, sets up a parallel field to the metal surface. More details can be found in the published works [3, 4, 18, 19]

## 2.3   Wireless Power Transfer Based Sensing

Wireless power transfer systems transfer maximum power when they are operating under resonance matched conditions[20]-[25]. As seen in the fig 2.7 , a disturbance in the resonance frequency on either Tx or Rx will lead to a drop in efficiency [23]. It is noteworthy that human body offers impedance, often known as human-body bio impedance [23],[26]-[35].

### 2.3.1   A. Generalized theory of Wireless Power Transfer Touch Sensing

In case of touch sensors the physical contact between finger/human hand/target object with the sensor head is registered. The use of wireless power transfer (WPT) systems as

**Impedance Matched : No Touch**



$$f_{RESONANCE} = \frac{1}{2\pi\sqrt{L_{Tx}C_{Tx}}} = \frac{1}{2\pi\sqrt{L_{Rx}C_{Rx}}}$$
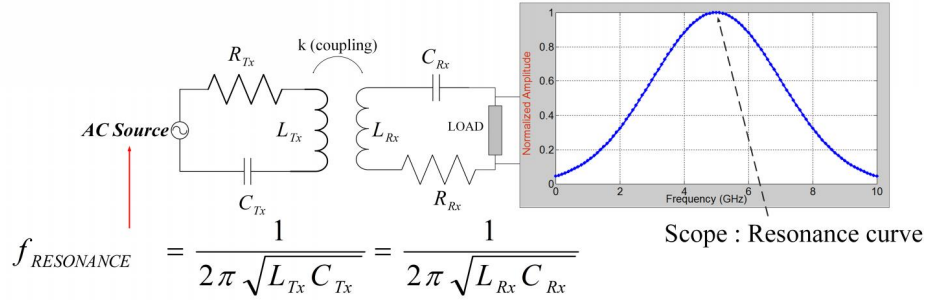
**Impedance Mismatch : Touch**



$$f_{RESONANCE} = \frac{1}{2\pi\sqrt{L_{Tx}C_{Tx}}} \neq \frac{1}{2\pi\sqrt{(L_{Rx}+L_{Body})\times(C_{Rx}+C_{Body})}}$$
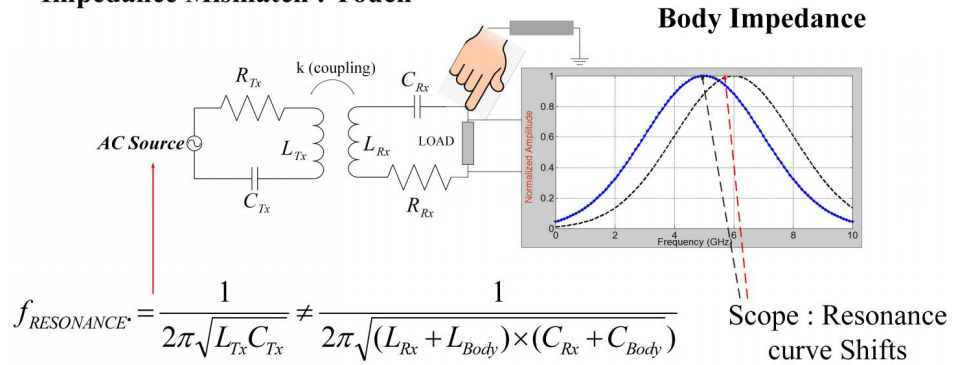
FIGURE 2.7: Impedance mismatch and resonance frequency peak shift due to bio-electrical parameters of human body [23].

touch sensors is a plausible alternative. The published work articulates the issues faced by existing touch sensors in details [23]. Which include range, linearity, conductivity of the target object and RC time constant delays faced by large contour display touch screen panels using the capacitive touch technology.

The WPT touch sensor can be modeled as a two port or three port network operating at resonance frequency. The measure of power transfer efficiency can be given by either S-21 oe S-31 , depending on the two port or three port system [23]. The resonance frequency equation is given by:

$$f_{Resonance} = \frac{1}{2\pi\sqrt{L_{Tx}C_{Tx}}} = \frac{1}{2\pi\sqrt{L_{Rx}C_{Rx}}} \tag{2.16}$$

After registering a touch the corresponding shift in the resonance frequency can be accounted for by the following equation:

$$f_{Resonance} = \frac{1}{2\pi\sqrt{L_{Rx}C_{Rx}}} \neq \frac{1}{2\pi\sqrt{(L_{Rx} + L_{Body})(C_{Rx} + C_{Body})}} \qquad (2.17)$$
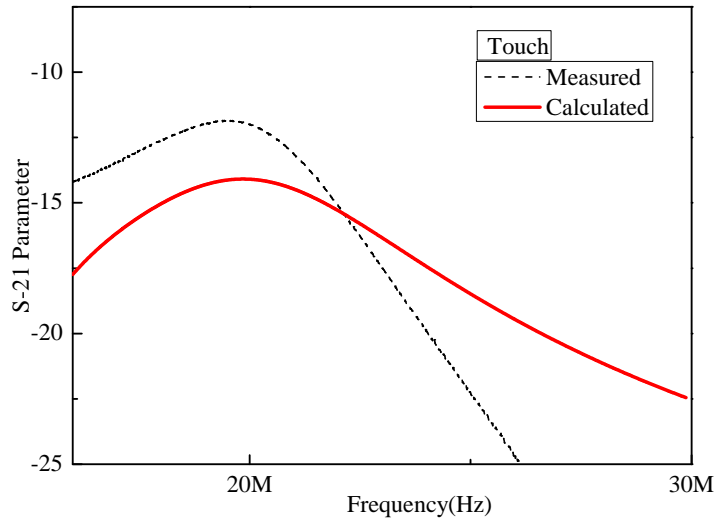


FIGURE 2.8: Measured and calculated values of touch sensing
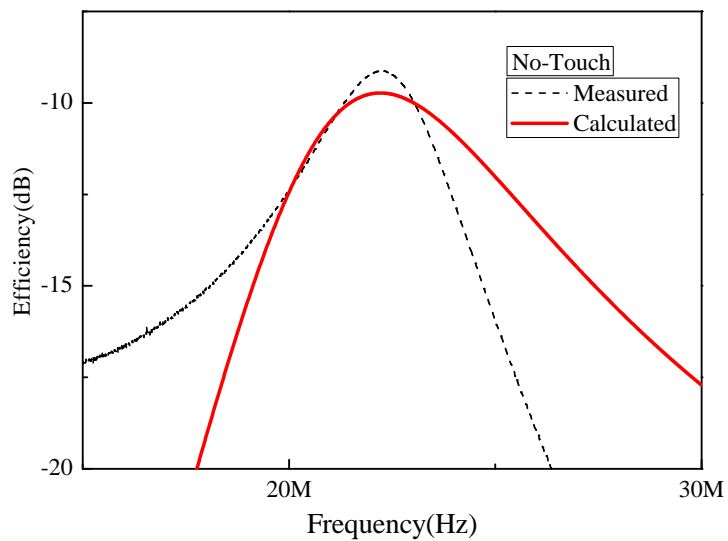


FIGURE 2.9: Measured and calculated values of touch sensing: No touch.

Its worth noting that in case when the frequency is in 10 to 50 megahertz range, the finger offers an impedance of 1000 $\Omega$ and human finger dielectric constant is in the range of 100-120 [23],[29]-[31].

## 2.3.2 Theory: Touch Mode

Fig.2.10 shows a cross-sectional view of the proposed Tx/Rx system in a touch sensing mode. It is assumed that the EM wave travels along the positive X axis, and only TM field invariant is considered for the sake of analysis, which follows from analysis presented in [19]. The Y components of the H field (complex amplitude) are normal to the top mesh layer. The upper limit of the Y component of the H field is at the insulation layer and Rx interface and the lower limit is at the top mesh layer of the Tx. The enclosed region in fig.2 accounts for the power flowing out of the Tx and the power being extracted and stored by the Rx. The power equation can be written as follows [24],[25]:

$$P_{AA'} = P_{BB'} + P_{AB} + P_{B'A'} + P_{Dissipation} \tag{2.18}$$

The components of interest in equation 2.18 are $P_{AA'}$ and $P_{BB}$ . It is worth noting that the power components $P_{A'B'}$ and $P_{AB}$ are lost, apart from $P_{Dissipation}$, which has been ignored for the sake of discussion. Hence, from the analysis presented in [19]-[25], the power under the enclosed regions and can be given as follows:

$$P_{wave-cavity} = \frac{1}{2} X_s \pi r_c^2 \iint H_{BB'}^y, H_{AA'}^y \sin\theta.dA \tag{2.19}$$

Where $X_s$ is the surface reactance of the Tx/Rx conductor plane,$r$ is the radius of the cavity, and $r_c$ is the inner radius of the cylindrical cavity. $X_s$ is expressed in the following form:

$$X_s = X_S' \sqrt{\frac{\mu}{\epsilon}} \tag{2.20}$$

Equation 2.20 implies that the surface reactance is equal to the inverse square root of the dielectric permittivity. This supports the previous claim that the dielectric constant of human skin affects the surface reactance of the WET system. Hence, the impedance offered by a human finger or hand should cause a change in $X_S$ in equation 2.19. Thus, the change in the power equation can be written as follows:

$$\Delta P_{wave-cavity} \equiv \frac{1}{2}(\Delta X_s)\pi r_c^2 . \iint H_{BB'}^y H_{AA'}^y \sin\theta . dA \qquad (2.21)$$

Thus, based on the theoretical aspects considered in this sub-section, it should be possible to register the changes in the voltage and current levels due to the placement of human skin/finger directly over the receivers of the proposed system.
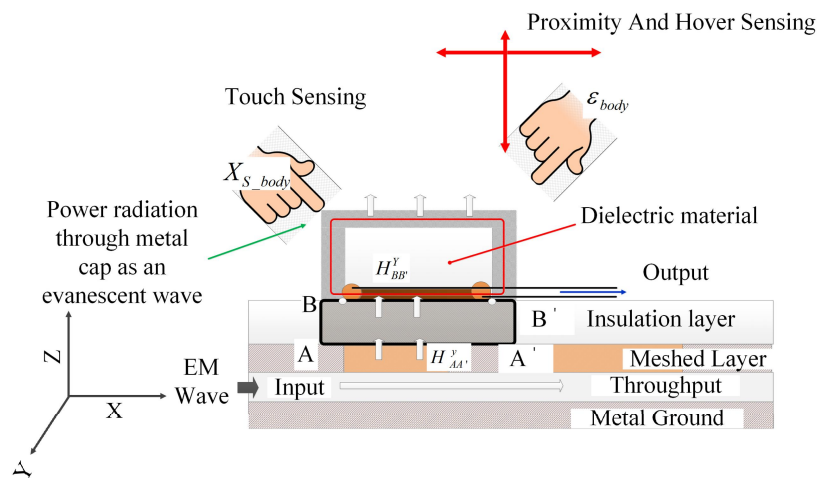


FIGURE 2.10: Operation Principle.

## 2.3.3 Theory : proximity and hover sensing modes

Fig.2.10 depicts the operation theory of the proposed system for proximity and hover sensing. As previously mentioned, the Tx of the proposed system generates an evanescent EM wave. Evanescent EM waves are generated at a metal-dielectric interface [36].

Likewise, a metal-dielectric interface is formed between the top metal cap and the dielectric material of the Rx, as seen in fig.2.10 .Thus, the energy equation for the evanescent part of the field [37] can be written as follows:

$$W_e^{evanescent}(\widehat{u}) = \frac{\epsilon}{4} \int_{volume} d^3r \left| E_{evanescent} \left[ r; \widehat{u(r)} \right] \right|$$
(2.22)

The change in the energy due to the permittivity $\epsilon$ offered by a human finger/hand can be accounted for using equation (14), as follows:

$$\Delta W_e^{evanescent}(\widehat{u}) = \frac{\Delta\epsilon}{4} \int_{volume} d^3r \left| E_{evanescent} \left[ r; \widehat{u(r)} \right] \right|$$
(2.23)

As the permittivity changes, the evanescent energy in equation 2.22 changes, this change can be accounted by equation 2.23.

Thus, based on the theoretical aspects presented in this sub-section, it should be possible to carry out proximity and hover sensing using the proposed WET system.

## 2.4 Summary

- *Surface Electromagnetic Wave.* Generated when an incident EM field undergoes a total internal reflection due to the metal present intimately to the EM field source.

- *Evanescent fields and Floquet's theorem at metal-air interface.*The EM field interacts with the altering crystalline grain and air voids at a microscopic level of the metal. If the EM field wavelength is much larger than the periodicity of metal grain-air void structures. This causes the setup of infinite evanescent modes and hence backward and forward propagating surface waves. This is accounted by Floquet's theorem.

- *Experimental Verification of Gerson and Nadan Model.* The experimental verification of Gerson and Nadan model showed excellent fit with the spectrum analyzer results.

# Chapter 3

# Transmitter and Receiver Design

## 3.1 Resonance frequency Sheet-like waveguide Cylindrical Wave cavity receiver

The details of the design of cylindrical wave cavity receivers has already been described well in [3] and [4]. The focus of this thesis is to determine an approximate analytical equation. In the near-field wireless systems, the resonance frequency is largely dependent on the physical dimensions of the transmitting and receiving antenna or in other words, area.

$$f_{resonance} = \frac{c \times t_{coppercoil}}{\epsilon_r Area} \tag{3.1}$$

In the equation 3.1, $t_{coppercoil}$ is the thickness of the copper coil in the cylindrical wave cavity receiver. $c$ is the speed of light in $m/s$. The quantity $Area = \pi r^2$ which is the area occupied by the receiver. The quantity $\epsilon_r$ is the relative permittivity of the dielectric used. The details of the design are depicted in figure 3.1.
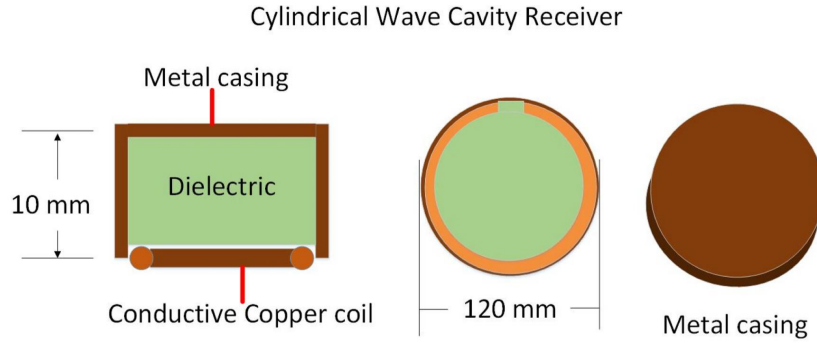
FIGURE 3.1: Cylindrical Wave Cavity Receiver.

## 3.2 Sheet like waveguide Transmitter-Receiver

### 3.2.1 Inductance

The inductance of the top layer of the sheet was calculated by the following modified empirical impedance model presented in [38]:

$$X(f)_{ind} = 7.1124 \times 10^4 \frac{gf}{kc} \left[ \csc\left(\frac{\pi a}{g}\right) \right] \tag{3.2}$$

Where $c$ is the speed of light, $f$ is the frequency, $k$ is an unknown constant, assumed to be unity in the present case, $g$ is the mesh period as shown in figure 3.2, the extracted inductance value can be represented by $L_{mesh}$

The inductance of the mesh layer with intermediate layer is given by the equation:

$$L_{m-i} = 2 \times 10^{-4} l_G \left[ Q_1 + Q_2 \right] \left[ \mu H \right] \tag{3.3}$$
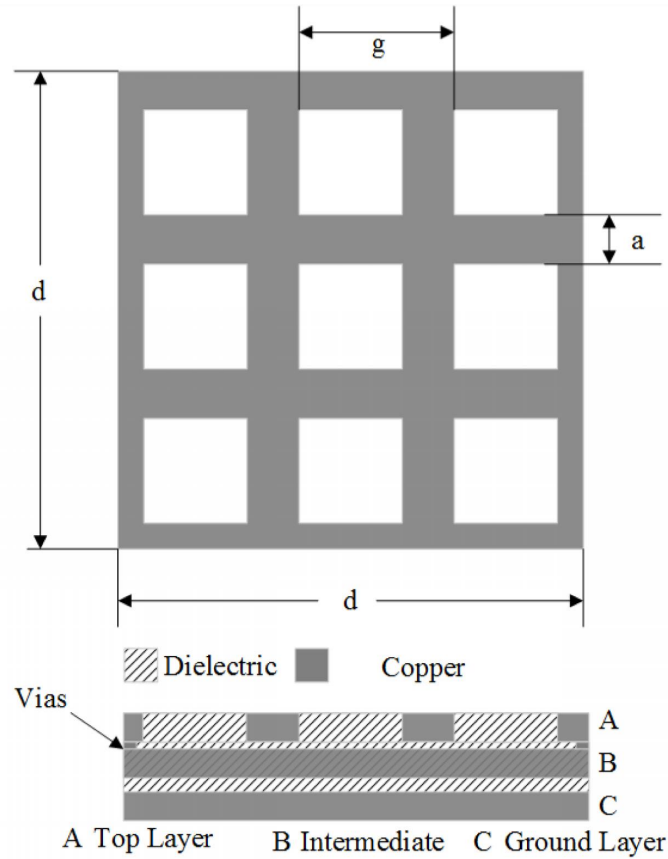
FIGURE 3.2: Sheet like waveguide details.

where $Q_1 = log\left(\frac{2l_i}{W_i+t_i}\right) 0.5$ and $Q_2 = 0.2335\left(\frac{W_i+t_i}{l_i}\right)$. Where, $l_G$ is the ground layer length and $t_i$ is the ground layer thickness, $W_i$ is the ground width.

The inductance of the ground layer with intermediate layer is given by the equation:

$$L_G = 2 \times 10^{-4} l_G \left[S_1 + S_2\right] \left[\mu H\right] \tag{3.4}$$

where $S_1 = log\left(\frac{2l_G}{W_G+t_G}\right) 0.5$ and $S_2 = 0.2335\left(\frac{W_G+t_G}{l_G}\right)$. Where, $l_G$ is the ground layer length and $t_G$ is the ground layer thickness, $W_G$ is the ground width. The total inductance of the transceiver can be given by $L_{Tx-Rx} = L_{mesh}||L_{m-i}||L_G$.

## 3.2.2 Capacitance

The capacitance of the transmitter $C_{Tx}$ has two components: the mesh to intermediate conductive copper layer given by $C_{mesh\mathbf{int}}$ and the intermediate layer to ground capacitance given by $C_{int\mathbf{gnd}}$

$$C_{Tx} = \left[ \frac{\left(\epsilon_r \epsilon_0\right)^2 \frac{A_{mesh}}{t_{mesh\mathbf{int}}} \frac{A_{int\mathbf{gnd}}}{t_{int\mathbf{gnd}}}}{\epsilon_r \epsilon_0 \frac{A_{mesh}}{t_{mesh\mathbf{int}}} + \epsilon_r \epsilon_0 \frac{A_{int\mathbf{gnd}}}{t_{int\mathbf{gnd}}}} \right] \tag{3.5}$$

$A_{mesh}$ is the mesh area of the top layer which is shown in fig. 3.2, the complete sheet like waveguide transmitter structure is also shown , which demarcates the distinct structure of the transmitter. Likewise the parameter $A_{int\mathbf{gnd}}$ is the area of the intermediate and ground layer. The parameters $\epsilon_r$ and $\epsilon_0$ are the relative and free space permittivity respectively.

## 3.2.3 Capacitance link between Transceivers and Metal

Presence of metal play a vital role in the determination of resonance frequency. The transceivers are placed directly over the metals with an insulation layer of 0.5 $mm$ thickness, in order to avoid an electrical contact between the transceivers and the metal. This forms a capacitance between transceiver and the metal. By assuming the parallel plate capacitance effect, the metal-transceiver capacitance can be calculated by:

$$C_{Metal-TX} = \epsilon_r \epsilon_0 . \frac{A_{metal-TRX}}{t_{insulation}} \tag{3.6}$$

Where $C_{Metal-TX}$ and $C_{Metal-RX}$ is the capacitance between metal-transmitter and metal-receiver respectively. $t_{insulation}$ is the thickness of the insulation between metal and transceivers. $A_{metal-TRX}$ is the area of overlap between transmitter and metal or receiver and metal. Also, $C_{Metal-TX} = C_{Metal-RX}$

### 3.2.4 Inductance and resistance of the metal

The inductance of the metal can be modeled using the following equation :

$$L_{Metal} = 2 \times 10^{-4} l_M \left[ S_{1M} + S_{2M} \right] [\mu H] \tag{3.7}$$

where $S_{1M} = log\left(\frac{2l_M}{W_M + t_M}\right) 0.5$ and $S_{2M} = 0.2335 \left(\frac{W_M + t_M}{l_M}\right)$. Where, $l_M$ is the metal length and $t_M$ is the metal thickness, $W_M$ is the metal width.

The resistance can be given by the equation :

$$R_{metal} = \frac{\rho l_M}{t_M W_M} \tag{3.8}$$

### 3.2.5 Resonance Frequency Determination

We propose an equation to determine the resonance frequency. Since the transceiver operation is based on evanescent fields, which are a part of the reactive near field component, the resonance frequency will be dependent on the physical dimensions of the transceiver. An approximate equation for this relation could be given by the following:

$$f_{resonance} = \frac{A' \times t_{total}}{\sqrt{\mu_0 \epsilon_0} \epsilon_r Area} \tag{3.9}$$

The effective value of $\epsilon_r$=1.67 to 3 and $A'$ is the unknown dimensionless constant.Hence, at a given area of 0.0225 $m^2$, $t_{total}$ is the transceiver thickness, $0.003m$, and the resonance frequency is 13.33 MHz. The measured and calculated frequency and area dependence has been listed in table 3.1 The details of inductance and capacitance are shown in fig. 3.3, four prototypes for four different resonance frequencies were built to validate the equation 3.9 . In order to validate the effectiveness of this handy equation 3.9, we compare it with software based calculation and experimental results, using Agilent 's Advanced system design software (ADS) .

TABLE 3.1: Frequency and Area

|  | Area ($mm^2$) | Calculated(MHz) | Measured(MHz) |
|---|---|---|---|
| Prototype 1 | 112 | 25 | 25.01 |
| Prototype 2 | 144 | 20.83 | 20.9 |
| Prototype 3 | 225 | 13.33 | 13.08 |

## 3.2.6 Advanced system design model for resonance frequency and experimental results

**Sheet Like Waveguide Transmitter and Spiral Coil Receiver**

From the equations 3.2 to 3.6 the equivalent inductance and capacitance values can be determined, these values have been listed in table 3.2. The spiral coil parameters were determined using standard equations, not shown in this work. The coil turn n=12.5, average winding radius =1.37 inch, width of winding=1.15 inch.

**Sheet Like waveguide Transmitter and Receiver**

From the equations 3.2 to 3.6 the equivalent inductance and capacitance values can be determined, these values have been listed in table 3.3. These values were used on ADS to calculate the S-21 parameters. The topology of the equivalent circuit used on ADS is shown in fig. 3.4. The transmitter and receiver are coupled only to the metal, there is no coupling between receiver and transmitter in the presented model. The value of coupling $k$ has been assumed to vary between 0.63 and 0.64.

## 3.2.7 S-parameter: Equivalent Circuit Model-I

The case of sheet like waveguide transmitter-receiver is considered in this section, in order to validate the equation 3.9, three cross-checks were performed. (i.) the calculated value of the resonance frequency from the equation 3.9, (ii.) the simulated ADS
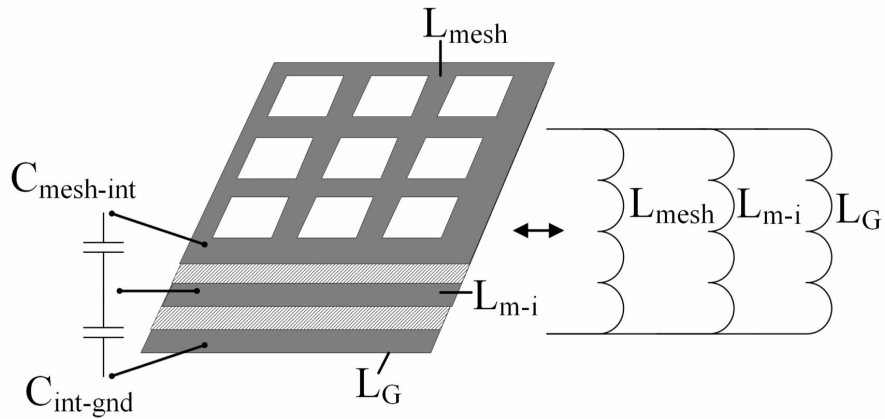
FIGURE 3.3: Sheet like waveguide: Capacitance and Inductance.

TABLE 3.2: Transmitter : Sheet like-waveguide, Receiver: Spiral coil

| Parameter | Value |
|---|---|
| Sheet like waveguide transmitter | |
| Inductance from equation 3.2 | 1.9833 $\mu H$ |
| Inductance $L_{m-i}$ | 4.2 $nH$ |
| Inductance $L_G$ | 4.2 $nH$ |
| Capacitance $C_{Tx}$ | 289.2 $pF$ |
| Transmitter $L_{Tx}$ | 1.02$\mu H$ |
| $R_{Tx}$ | 250 $m\Omega$ |
| $C_{Metal-TX}$ | 322.7 $pF$ |
| Spiral Receiver | |
| $L_{Rx}$ | 12.6$\mu H$ |
| $C_{Rx}$ | 6.02$pF$ |
| $R_{Rx}$ | 25$m\Omega$ |
| $C_{Metal-Rx}$ | 25.02$pF$ |
| $\epsilon_r$ | 1.67 to 3 |
| $L_{Metal}$ | equation 3.7 |
| $R_{Metal}$ | equation 3.8 |
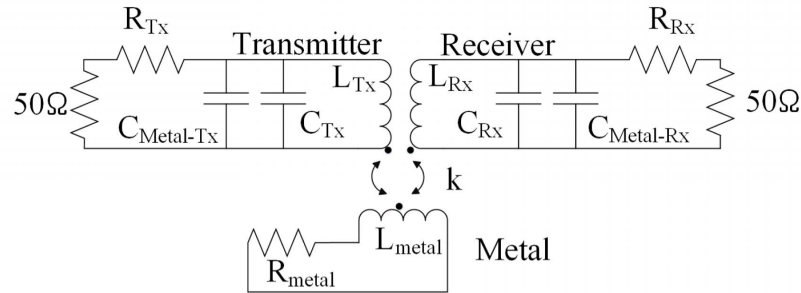
FIGURE 3.4: Equivalent circuit: ADS model.

TABLE 3.3: Sheet like waveguide Transceiver parameters

| Parameter | Value |
|---|---|
| Inductance from equation 3.2 | 1.9833 $\mu H$ |
| Inductance $L_{m-i}$ | 4.2 $nH$ |
| Inductance $L_G$ | 4.2 $nH$ |
| Capacitance $C_{Tx} = C_{Rx}$ | 289.2 $pF$ |
| $L_{Tx-Rx}$ | 1.02 $\mu H$ |
| $C_{Metal-TX} = C_{Metal-RX}$ | 322.7 $pF$ |
| $\epsilon_r$ | 1.67 to 3 |
| $L_{Metal}$ | equation 3.7 |
| $R_{Metal}$ | equation 3.8 |
| $R_{Tx} = R_{Rx}$ | 250 $m\Omega$ |

model , and (iii.)the measured S-21 parameter peak as shown in fig3.5. The equation 3.9 yielded a value of 13.33 MHz, while the ADS model (values taken from table 3.3)yielded somewhat a flat peak. The calculated max peak exists at 13.64 MHz and the measured value settled around 13.07-13.08 MHz. The ADS model assumes ideal conditions, where as the real working scenario is very different, and hence the ADS model has limitations. All the above three cross-checks point towards the reliability of the equation 3.9 and hence a complicated rigorous model for surface wave theory can be bypassed for any practical design purposes. Despite of the limitations, the presented ADS model considers the inductance offered by the metal to be a variable of the distance between transmitter and receiver. This implies that the inductance increases as
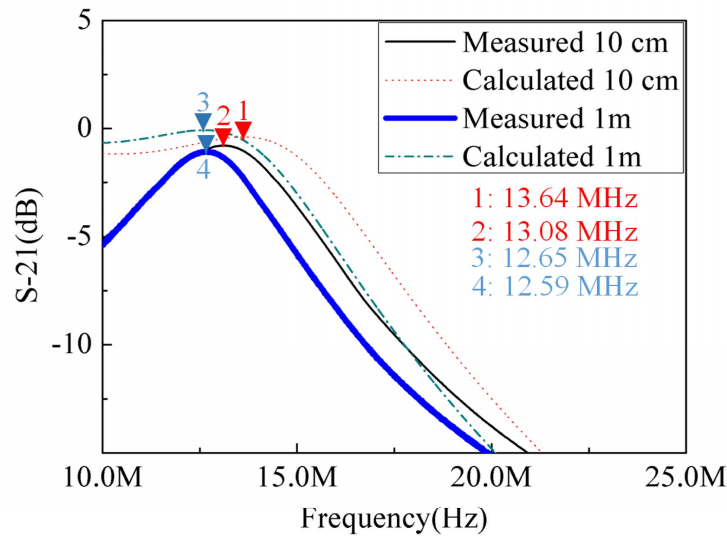
FIGURE 3.5: Left shift of peaks as the distance between transmitter and receiver increases: calculated (markers 1& 3) and measured (markers 2&4) values. Markers 1 &2 for 10 cm distance and markers 3 &4 for 1 m distance.

one places the receiver far apart from the transmitter (while, placing them intimately to the metal). This rise in inductance should cause the S-21 peak to shift towards the left, i.e. rise in the resonance frequency. This phenomenon has been validated with the measured results in fig. 3.5. The measured value of the shift in the peak appears at 12.59 MHz, while, the ADS-calculated value appears at 12.65 MHz for 1 meter distance between the transmitter and receiver.

There is however one limitation of this model, when the distance between the receiver and metal is increased, the capacitance value $C_{Metal-Rx}$ goes down, this causes the resonance peak to shift towards the right as per the relation $f = \frac{1}{2\pi\sqrt{LC}}$. However, when the measurement is done on network analyser, there exists no peak. The values of S-21 parameters decay exponentially with respect to the vertical distance between the metal and the receiver.

### 3.2.8 S-parameter: Equivalent circuit model-II

The equivalent circuit model-II is more realistic model. The curve fit plot of mutual inductance values $k23$ values have been shown in fig 3.6 at 10 cm distance between transmitter and receiver, when placed intimately over the metal with an insulator of 0.5 mm thickness. It was mentioned in the previous sub-section that the model-I have limitations to predict the outcome of the case, when receiver is moved vertically away from the metal. As seen in fig 3.7, the difference between measured and calculated values at 13.08 MHz is more than 20 $dB$ for model-I and measured. In fact, the model-I and II results exhibit a peak towards the high frequency side. However, more details are revealed when the S-21 peak values are plotted when the distance between the receiver and the metal is varied from 0.5 to 5 $mm$. As seen in fig 3.8, the model-II closely mimics the exponential decay as observed in the measured values.
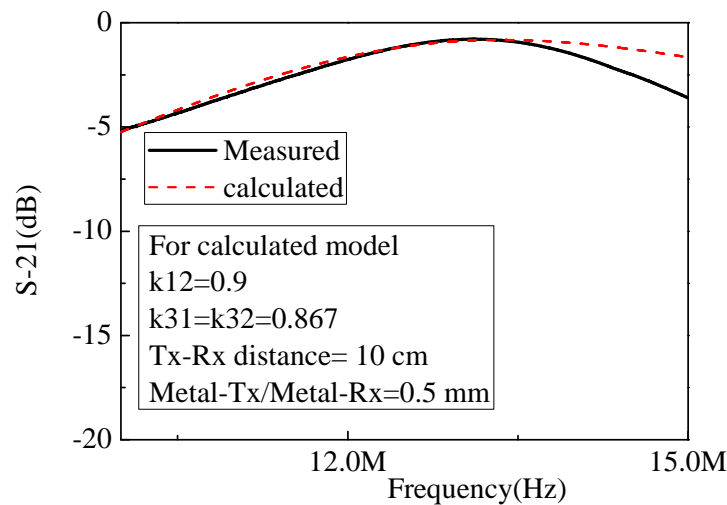


FIGURE 3.6: Data fit for mutual inductance $k23$ at 10 cm distance between transmitter and receiver: Model-II .

### 3.2.9 Model-II: Coupling coefficient $k23$, distance and $S - 21$ peaks

It is important to get an insight into the change in the values of coupling values $k23$ with respect to vertical distance variation between receiver and metal. The table 3.4
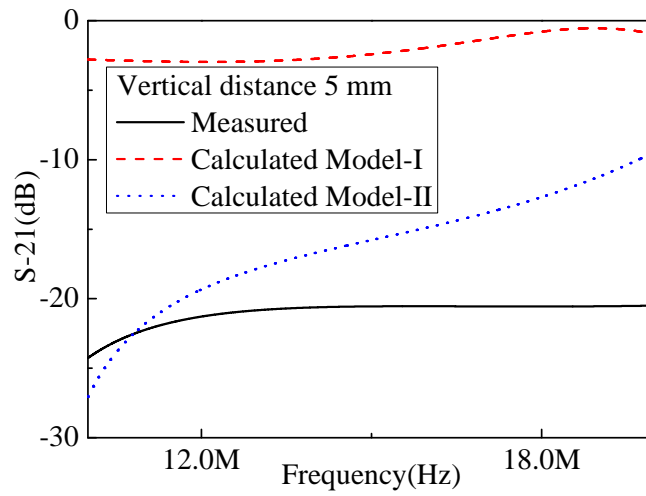
FIGURE 3.7: Data fit for mutual inductance $k23$ at 5 mm distance between metal and receiver for: Measured, Model-I and Model-II .
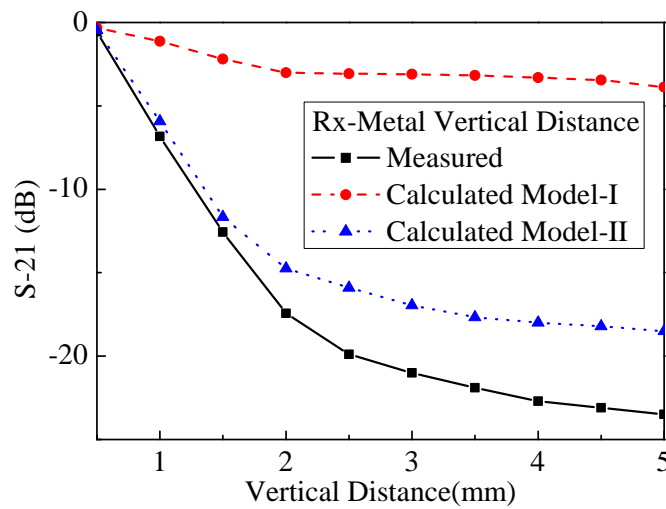


FIGURE 3.8: Plot of $S21$ peak values vs distance between metal and receiver varied from 0 to 5 mm: Measured, Model-I and Model-II.

shows the details. These values show that the assumed equivalent circuit model-II is suggesting a close agreement with the experimental values.

TABLE 3.4: Model-II : $k23$, distance and $S - 21$ Peaks at 13.08 $MHz$

| $k23$ | Vertical Distance(mm) | Calculated (dB) | Measured (dB) |
|---|---|---|---|
| 0.87 | 0.5 | -0.089 | -0.092 |
| 0.35 | 1 | -6.92 | -7.12 |
| 0.002 | 2 | -14.5 | -17.82 |
| 0.001 | 5 | -18.41 | -22.39 |

## 3.3   Summary

### Power and Data

- *Resonance Frequency.* Dependent on physical dimensions, inversely proportional to the area of the transmitter-receiver. It is noteworthy that the sheet like waveguide transmitter does not show a resonance unless the receiver is brought in close proximity. This also implies that the resonance frequency of the receiver under question governs the resonance frequency heavily.

- *Sheet like waveguide parameters.*Inductance, Capacitance and resistance of the sheet like waveguide has been calculated using the empirical equations 3.2 to3.8

- *Capacitance Between Transceiver and The Metal.* This is dependent on the physical area of the transceivers.

- *Equivalent circuit Model.* The equivalent circuit model considers the coupling of the transmitter and receiver with the inductance offered by the metal.

- *S-21 Parameter.* The S-21 parameter peak shifts towards the right as one increases the distance between the transmitter and receiver, while they are placed intimately to the metal. This shift is observed because the inductance offered by the metal is

a function of the distance between the transmitter and the receiver.

## Sensor

- *Resonance Frequency of The Sensor* The sensor head used in this work is the wave cavity receiver, whose resonance frequency can be determined using the equation 3.1.

- *Parameters of the transceivers*The same equations 3.2 to3.8 can be used to determine the parameters. However, in this case one does not need to consider the metal.

# Chapter 4

# Results and Discussions

## 4.1 Power and Data Transfer

This section presents the results for the wireless power/data transfer through/via metal walls, obtained from the experiments which were conducted to confirm the theory presented in the previous chapters.

### 4.1.1 Sheet-like waveguide transmitter and cylindrical wave cavity receiver across open metal sheets

Fig.4.1 demonstrates the power transfer from the sheet-like waveguide Tx to the CWC Rx, across GI metal sheets upto 22.5 mm. An insulation spacer composed of polypro-plylene of 25 mm thickness is placed to avoid contact between the Rx and the metal wall. A 10 V peak to peak sinusoidal voltage at 25 MHz is fed into the Tx. The resulting output voltage of 3.98 V DC is obtained.
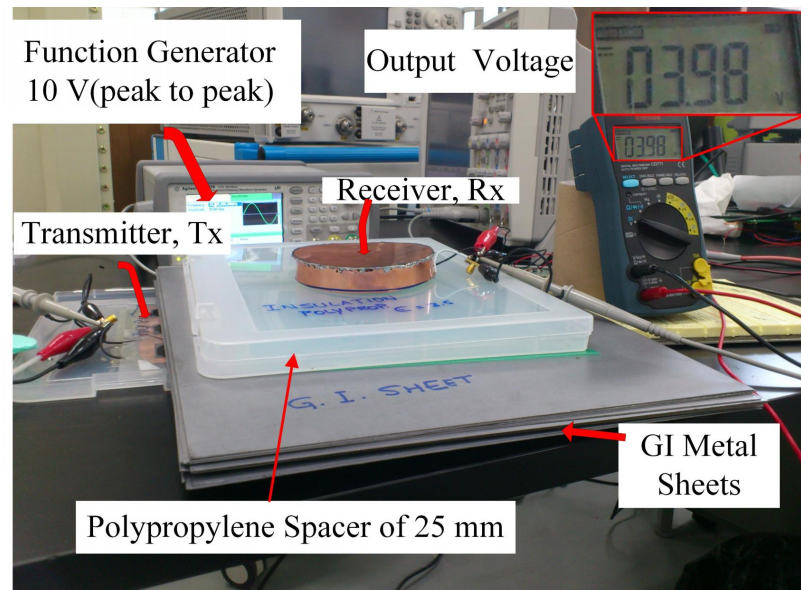
FIGURE 4.1: A DC voltage of 3.89 V was obtained on the CWC Rx side.

### 4.1.2 S-21 parameters for Sheet-like waveguide transmitter and cylindrical wave Cavity receiver across open metal sheet

The S-21 parameter is the measure of efficiency, and they are obtained experimentally using the network analyzer. Fig.4.2 shows the measured power transfer efficiency (S21-parameter) for the non-shielded, 1.5 mm shield, 10 mm shield and 22.5 mm shield cases. The values of the S-21 parameter for the different cases were -3.67,-3.7, 3.74 and -3.76 dB, respectively. The results confirmed the assumption that the overlying metal sheet do not absorb the power being generated by the proposed sheet-like waveguide.

### 4.1.3 Performance of cylindrical cavity receivers in the presence of partial enclosures

In the case of a sheet-like wave guide Tx and cavity Rx, the signal generator feeds a 10-V peak-to-peak sinusoidal voltage at 25 MHz, and the corresponding full wave rectified signal is read using a multi-meter.
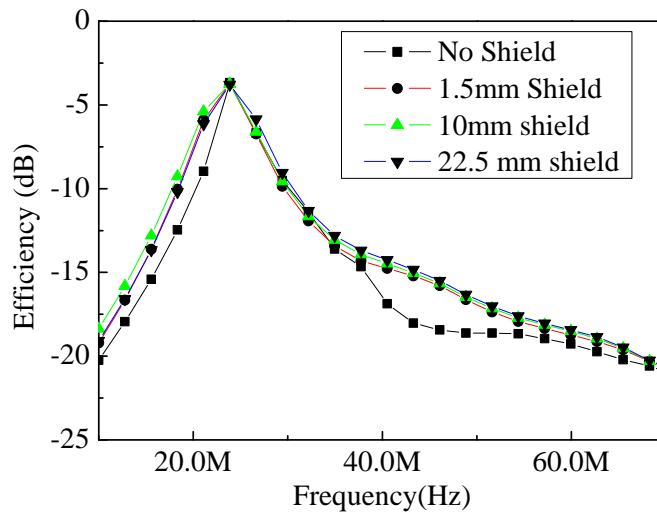
FIGURE 4.2: S21- parameters of the cylindrical wave cavity receivers (no shielding and with 1.5 to 22.5 mm thickness).
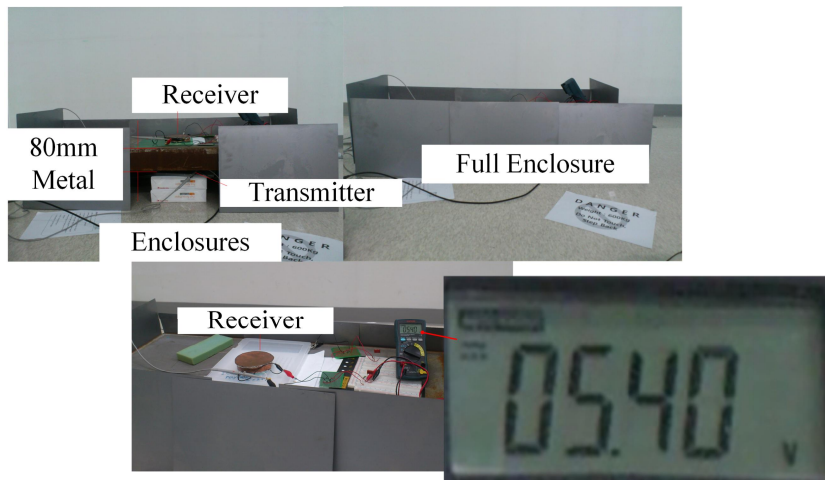


FIGURE 4.3: [Sheet-like waveguide transmitter and CWC receiver, across 80 mm ship metal block, in the presence of metal enclosure] Sheet-like waveguide transmitter and CWC receiver, across 80 mm ship metal block, in the presence of metal enclosure.

Fig.4.3, experimentally demonstrates the use of the sheet-like wave guide Tx and wave cavity Rx for 80-mm-thick metal wall. In this experiment a weak enclosure was used, and there were still large number of gaps for the EM wave to travel on the surface of the metal block and appear on the receiver. However, when the same setup is subjected to faraday shielding box, no signal is observed on the receiving end. This simply implies that this design does not work as desired under perfectly enclosed conditions

### 4.1.4 Sheet-like waveguide transmitter and spiral coil receiver

In the case of the sheet-like wave guide Tx and spiral coil Rx, a power amplifier was used as a power source at 25 MHz. The spiral coil receiver demonstrated a stronger magnetic linking capability, as seen in Fig 4.4(a)and(b). The experimental demonstrations shown in Fig.4.4 (a) and (b) are indicative that, as long as there is even a minute opening in the metal wall, due to the forward and backward waves which are set up due to infinite evanescent modes, it is possible to transfer power/data across metal walls.

For example the ventilation ducts in ships and the spacing created by the insulation between the ship walls and ventilation ducts and pipes. The fig.4.4 (a) is the demonstration of 14 watts load illumination. The power transfer efficiency performance indexes will be covered in a later part in this section.

Power transmission up to 400 cm (4 meters) was achieved as demonstrated in the fig.4.4(b). It is worth noting that a slight variation in the LED intensity was observed with respect to distance between Tx and Rx. To measure the variations in power an energy meter was used at the Tx and Rx.

### 4.1.5 Efficiency and resonance frequency system

Fig.4.5 shows the measured and calculated S-21 parameters for a distance of 20 cm between Tx and Rx, while placed close to the metal surface. More details on the calculations are presented in the later part of this subsection. Fig.4.6 shows the left shift in S-21 peaks as the distance between transmitter and receiver is increased, while keeping them intimately to the metal surface. The distance between the Tx and Rx was varied

a   Transmitter with insulation
b   Receiver with 14 Watt LED
c   Counterpoise
d   Ship Metal Block of 80 mm

(a)

e   280 mW

f   GI metal sheets   g   400 cm

(b)
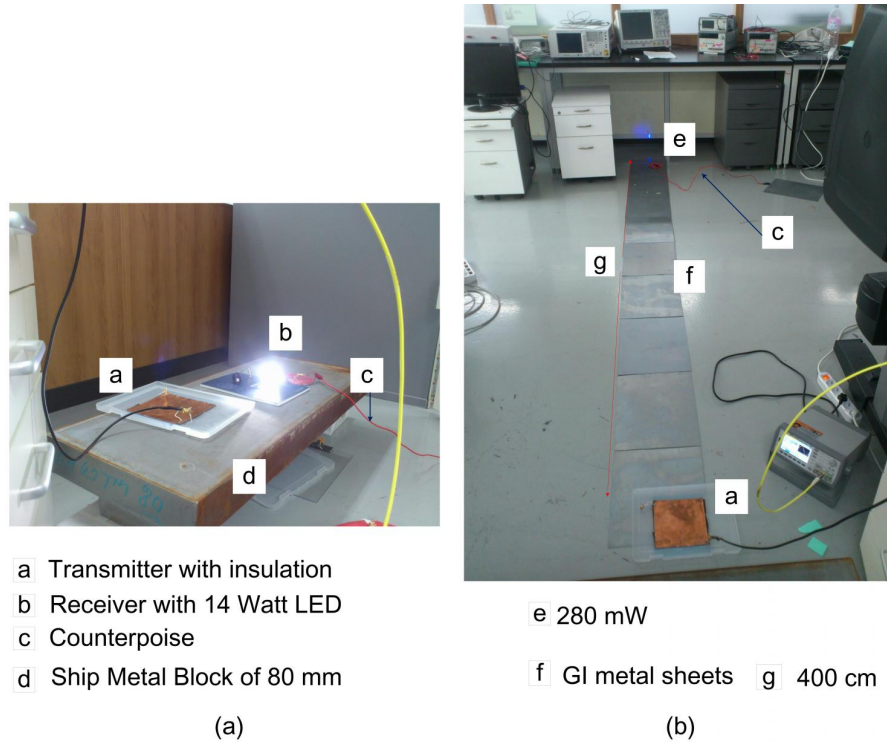
FIGURE 4.4: Power Transfer Demonstration(a)14 watts freely placed (b)280 mWatts across 400 cm.

between 10 cm and 400 cm. The characteristic exponential decay of the received power in the normal direction to the metal surface can be seen in 4.7. Fig4.8 shows the plot for the measured power transfer efficiency over the metal distance from 10 to 400 cm.

The supplementary material demonstrates the power transfer concept by illuminating a load of 280 mW across 4 m and a load of 14 W at arbitrary positions and across an 80-mm-thick metal wall. The equivalent circuit was calculated using Agilent Advanced System Design computer software in order to confirm the validity of the proposed circuit. All the parameters are listed in table 3.2, and were used for performing the simulation. The values of the coefficients of coupling were determined by curve-fitting between the experimental and simulation results.
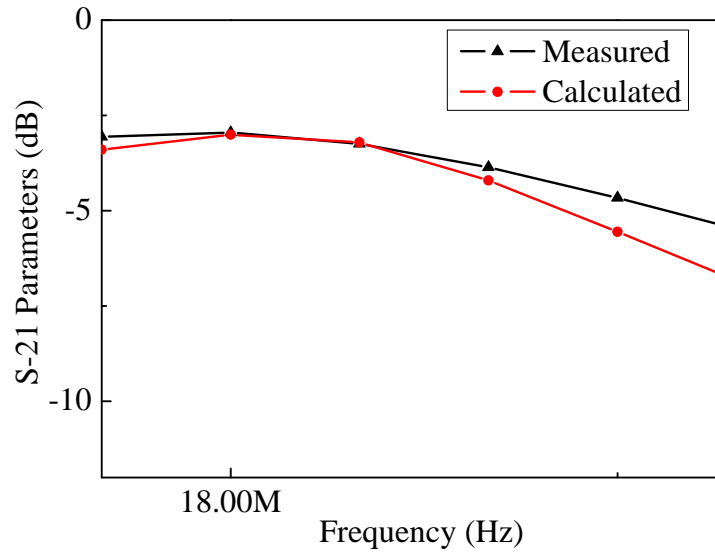
FIGURE 4.5: Experimental and calculated S-21 parameters.
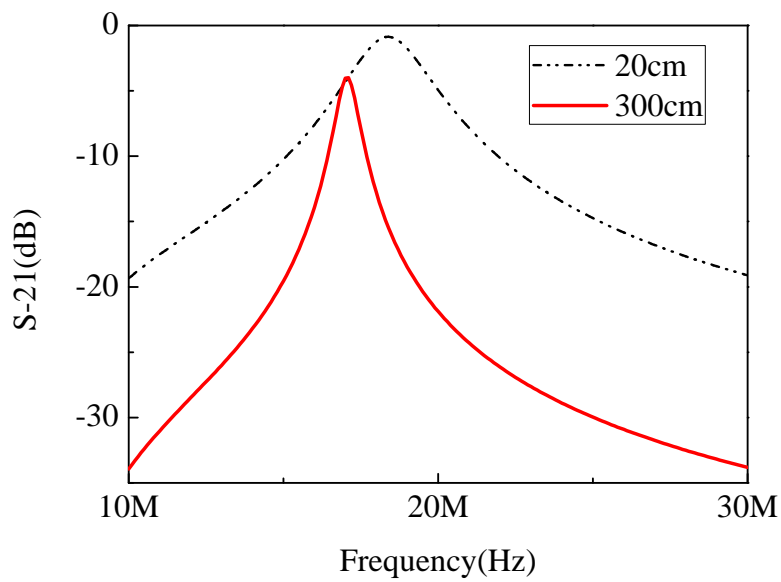


FIGURE 4.6: Measured S-21: Peak Shift towards the left, as one increases the distance between the Transmitters and Receivers.
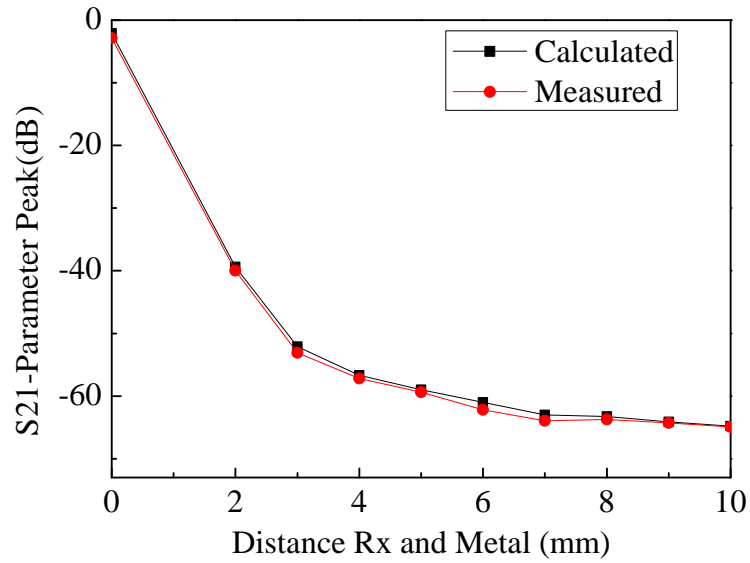
FIGURE 4.7: Calculated and Measured S-21 parameters on the receiver normal to the surface of the metal.
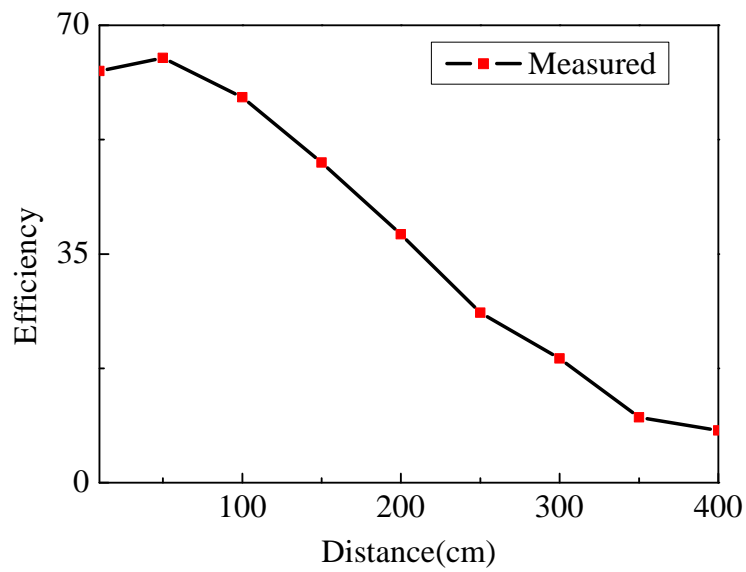


FIGURE 4.8: Measured Power Transfer Efficiency vs distance between transmitter and receiver.

## 4.1.6 Limitations of the equivalent circuit model

For distances greater than 100 cm, there exists a considerable difference between the calculated and measured power transfer efficiencies, because the proposed equivalent

circuit does not account for the eddy current losses . However, the calculated and measured values maintain a similar profile. Since the distances are too large, it is hard to calculate the eddy current losses. However, the approximate eddy current losses are given by a modified Dulnop relation[39] :

$$P_E \approx \frac{\pi^2 d^2 f^2 B_m^2 (l_{tx\_rx} \times t_{metal} \times d)}{16\rho} \qquad (4.1)$$

Here, $d$ is the receiver coil diameter, $f$ is the frequency, and $B_m$ is the peak value of magnetic flux. The variable $l_{tx\_rx}$ is the distance between the transmitter and receiver when placed on the metal, and $t_{metal}$ is the thickness of the metal.

## 4.2 Sheet-like waveguide transmitter and receiver system

The fig.4.9. shows the free positioning wireless power transmission design of the transmitter and receiver on a ship-grade steel block with a thickness of 80 mm. Fig.4.10 shows the power transmission over a distance of 400 cm. The load is 16 W in both fig.4.9 and fig.4.10. 40 Watt halogen load illumination demo video is listed in the supporting information section.

### 4.2.1 HFSS Simulation

Finite element method simulations using the ANSYS HFSS tool were performed to determine the H-field profile and existence of a surface wave in the case of a sheet-like waveguide transceiver system. Fig.4.11 shows the surface wave simulation. As seen, the H-field profile is in the range of 0.10758 $\mu$A per meter in fig.4.11 (a), and it is clearly evident that the spiral coil transmitter and spiral coil receiver setup are unable to transmit or receive signals. On the other hand, the H-field profile in fig.4.11 (b) is on the order of 3.247-3.5425 A per meter, and a surface wave is clearly seen being transmitted from the transmitter to the receiver.

FIGURE 4.9: Power transfer demo: free position.
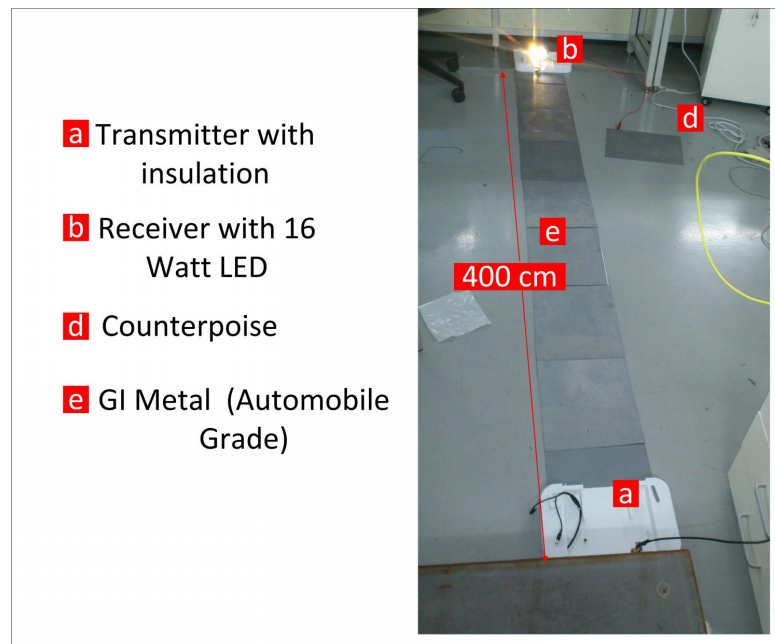


FIGURE 4.10: Power transfer demo: 400 cm distance.
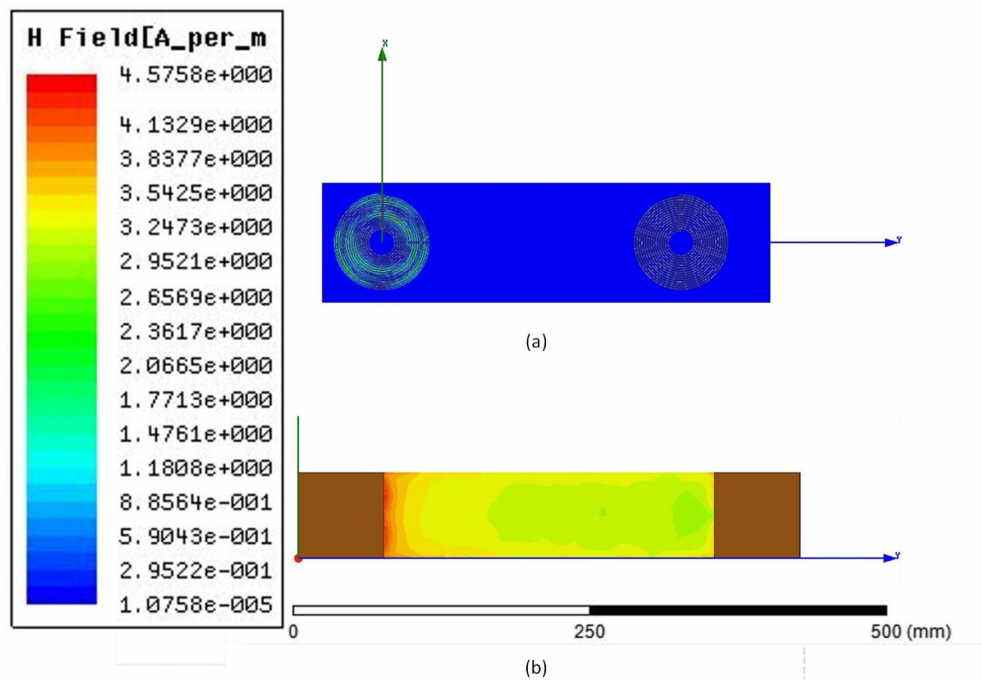
FIGURE 4.11: ANSYS HFSS Simulation (a) Spiral coil Tx and Rx (b) Sheet like waveguide Tx and Rx.

## 4.2.2 Power and Radio Transmission

The experimental setup of the power and radio transmission has been depicted in the fig4.12 and 4.13. The free positioning capability of the power transmission across a ship grade metal of 80 mm thickness, 1.2 meter length and 0.5 m width was tested. Whereas, the radio transmission was performed in real time on a Dolphin semisubmersible oil rig at the Hyundai ship yard based in Ulsan. The radio used for the test was an ordinary citizen band width radio from Luiton electronics company. The maximum power of the radio was 4 watts. The prototype of the system has been shown in fig. 4.14.

A power transmission of both 16 and 40 watts was successfully performed as a free positioning system on the ship metal wall as per the setup shown in fig 4.12 (a) and (b) A power transmission of 16 Watts across 400 cm metal line was successfully performed. Whereas a power transmission of 40 watts was conducted across 1.2 meters, ( more in the supporting information).

Planar arbitrary position on steel wall    Across 80 mm thick steel wall



■ Insulator    □ Transmitter/Receiver    ■ Steel
(a)                                        (b)

FIGURE 4.12: Experimental setup power transmission (a) arbitrary position (b)across.



FIGURE 4.13: Experimental setup Radio transmission in real time on an oil rig.

The a successful noise free radio transmission was done within the engine room of the rig  200-300 meters.  Where as the noise free radio transmission from the water submerged pontoon tanks, as well as engine room across atleast five metal complex floors was also achieved, without any problems as per the test scenario shown in fig. 4.13.

FIGURE 4.14: Prototype: With antenna structure and 3D printed casing which houses the radio and battery.

It is worth noting that in the test scenario of fig. 4.13 a wireless radio had never been able to communicate and no cellphone signals reached from the oil-rig open deck to the inside of the engine room and keel tanks. Where as, the proposed device, is able to communicate without any issues across such metal complexes. To cross-check the shielding environment, a regular wireless walkie-talkie and a smartphone was also used, however, neither of the two devices were able to communicate in the presented test scenario of the oil rig.

### 4.2.3 Efficiency

The measured S-21 parameter shown by the proposed system is in the range of -0.87 dB at a distance of 10 cm between the transmitter and the receiver, placed intimately to the metal. The calculated value of the same from the ADS model was -0.043 dB. However, the S-21 parameters sometimes do not translate to the effective efficiency in real time in case of wireless power transmission [19].

In order to measure the power transfer efficiency, an energy meter was used on both the transmission and the reception end, the efficiency was calculated using the ratio of received power to transmitted power. The power transfer efficiencies for three different prototypes have been listed in fig 4.15
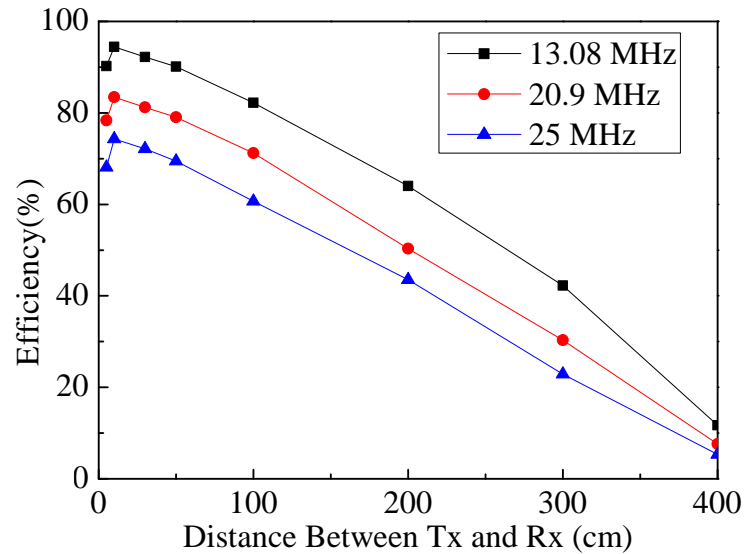


FIGURE 4.15: Efficiency plots of prototypes with three different frequencies with respect to horizontal distances between transmitter and receivers.

It is observed that at distance below 10 cm, there is a slight fall in the efficiency. In case of 13.08 MHz at 10 cm this efficiency is at the peak 94%. Where as beyond 10 cm the efficiency starts to gradually decline, the efficiency value between 100 and 200 cm declines from 82 to 64 % . Beyond 400 cm it is difficult to sustain wireless power transfer as the efficiency declines to 11%.

## 4.2.4   Differences in the Power and DataTransfer Efficiencies

It has been observed that the data transfer does take place over long distances without considerable drop in efficiencies. However in case of power transfer it is difficult to sustain power transfer efficiencies in the range of 12 to 10 % beyond 4 meters. This can

be accounted for by the saturation of iron/ steel due to frequency and power levels. This needs to be investigated further in future research.

## 4.2.5  Magnetic Flux Manipulation Method

The magnetic flux manipulation method feeds 10 V peak-to-peak at 20 MHz into the Tx through a metal enclosure with a thickness of 25 mm. The Tx and Rx were designed with the following parameters: L= 100 $\mu$H, turns = 70, R = 800 m$\Omega$, and  308 ampere-turns. A neodymium magnet with a diameter of 12.5 mm and height of 50 mm was used. A LabVIEW instrument control module was used to send a test amplitude-modulated signal to control a signal generator, which was read by using an oscilloscope on the receiving end. As an extension, the output of the oscilloscope on the receiving end was captured and demodulated by another notebook computer using a LabVIEW interface. Hence, wireless communication between two notebooks was established across fully enclosed metal walls.

The magnetic flux manipulation method requires axial alignment of the Tx and Rx. A decrease in the amplitude of the received signal was observed with a degree of mis-alignment.  Fig.4.16 experimentally demonstrates the magnetic flux manipulation by the transmission of a sine wave across a perfectly enclosed. Shielding box, which tries to mimic a ship hull.  Fig.4.17 depicts the AM signal transmitted across a perfectly shielded metal box. The magnetic flux manipulation method seemed to be a promising candidate for sending data across perfectly enclosed metal hulls with thicknesses of up to 25 mm.  In contrast, the sheet-like wave guide Tx with a cavity Rx or spiral coil Rx or sheet like waveguide Rx showed promising results for data and power transfer through ship ventilation systems, for an arbitrarily placed Tx and Rx. This freedom was somewhat restricted in the case of the magnetic flux manipulation method, as the Tx and Rx had to be aligned across the metal walls.Due to these reasons the magnetic flux manipulation method was not actively pursued any further.
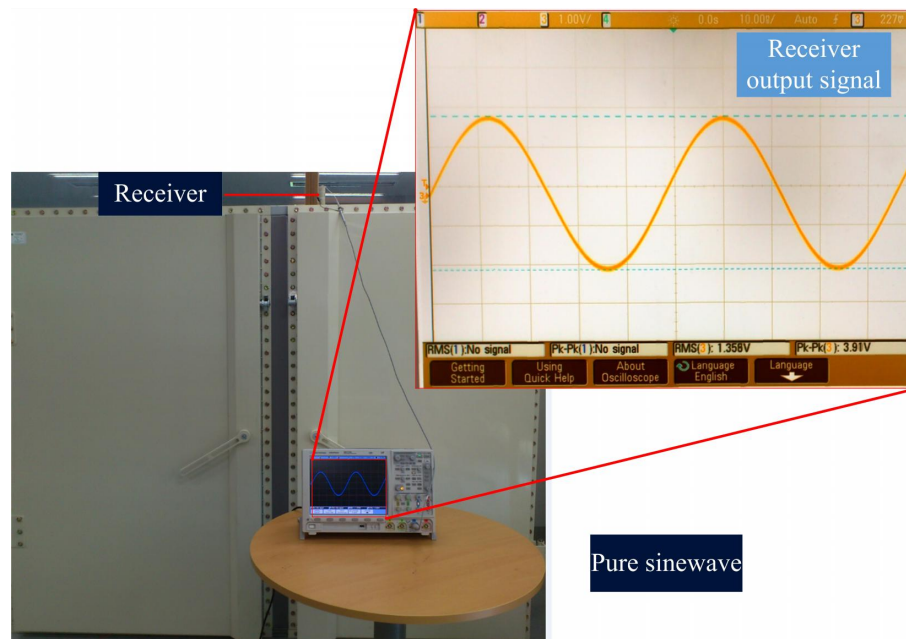
FIGURE 4.16: Magnetic flux manipulation method demonstration: Pure sine wave.

### 4.2.6 Voltage and Frequency characteristics of Magnetic Flux Manipulation Method

The fig.4.18 shows the measured values of output voltages w.r.t input voltages at 12, 20 and 25 MHz. The plot indicates towards the existence of higher efficiency at 20 MHz.

This section presents the results for the wireless power transfer based touch proximity and hover , obtained from the experiments which were conducted to confirm the theory presented in the previous sections.

## 4.3 Hover, Touch and Proximity Sensing

This section presents the results for the wireless energy transfer based touch, hover and proximity sensing, obtained from the experiments which were conducted to confirm the theory presented in the previous sections. Fig.4.19 shows the experimental setup used in this research.
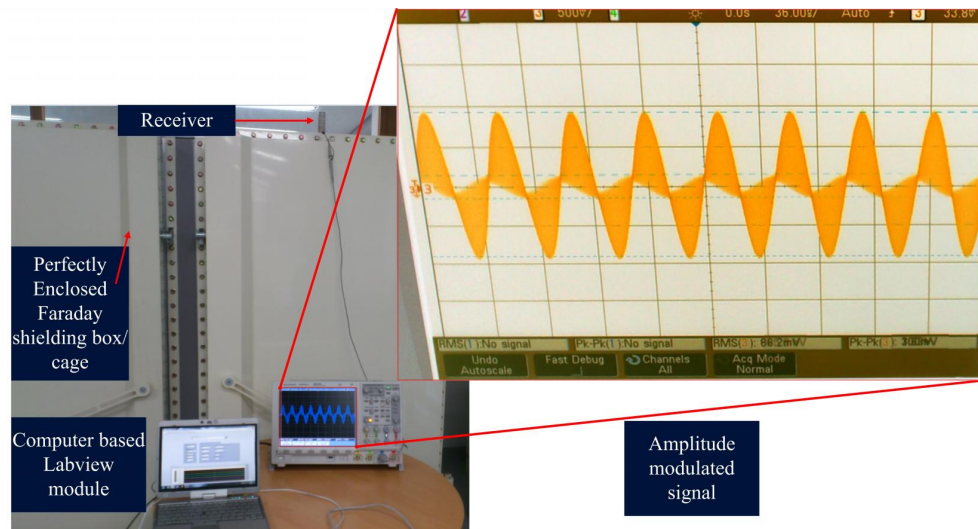
FIGURE 4.17: Magnetic flux manipulation method demonstration : amplitude modulated signal transfer.

### 4.3.1 S- Parameters Touch And No-Touch Experiment

For no touch condition the peak is observed at of -3.18 dBm at 29 MHz. More details on the theory of power transfer efficiency can be found in [10]. Shifts in the resonance peaks were observed upon touch, at 39.2 MHz. The power transfer curve obtained upon registering a touch also indicates lower value of S31 parameters, -8.37 dBm. Fig.4.20 shows the experimental setup used in this research. The S-31 parameters shown in fig.4.20 indicate the network analyzer experimental setup with the port notations and the power transfer efficiency vs frequency sweep plot for both touch and no touch

### 4.3.2 Sensitivity and Voltage Variations Experiment

Fig.4.21 and 4.22 shows sensitivity plots of the voltage changes with respect to the vertical and horizontal distances. Fig.4.23(a) shows the output voltage of 3.16 V on
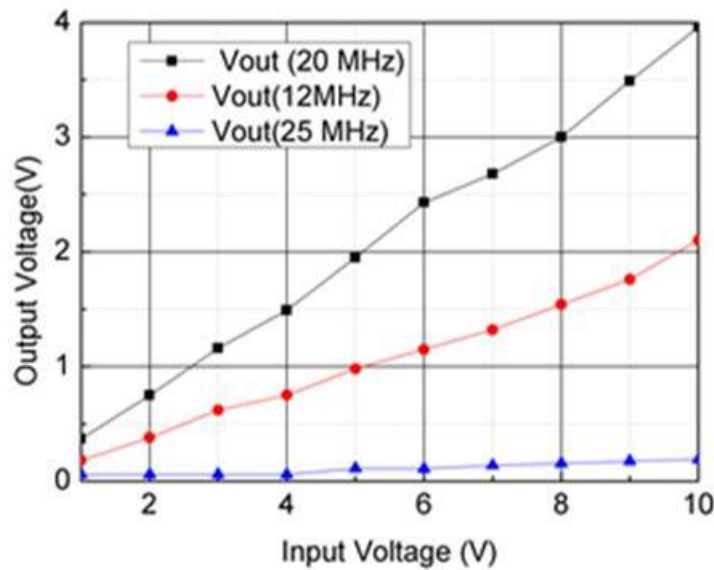
FIGURE 4.18: Magnetic flux manipulation: measured values of output voltage to input voltage at 12 MHz, 20 MHz and 25 MHz.

the Rx side obtained in the presence of a working LCD when no touch is registered. Fig 4.23(b) shows the variation of Rx output voltage as a confirmation of the touch mode theory shown in fig.3.x, the final value of output voltage is 2.11V upon touch. Fig.4.23(c) demonstrates the proximity in the presence of the LCD screen, the output DC voltage to confirm the theory presented in fig.3.x, the final output voltage on Rx side is 2.5V, when hand is at a height of 5 mm. In fig.4.23 (d) up to down hover motion is demonstrated to show the feasibility of the proposed system for hover motion sensing, when the hand is at a height of 5 mm. All these tests show that the presence of LCD screen doesn't affect the operation of the WET sensing system and vice versa.

### 4.3.3  Eddy Current and EMI Effects On LCD Screens

Additionally, two tests were conducted to evaluate (1) if there would be any effect of WET system on LCD performance. (2) If the WET system has any performance issues due to presence of electronic components in the overlapping region between the Rx and Tx. These results have been shown in fig.4.24. The presence of LCD screen between the
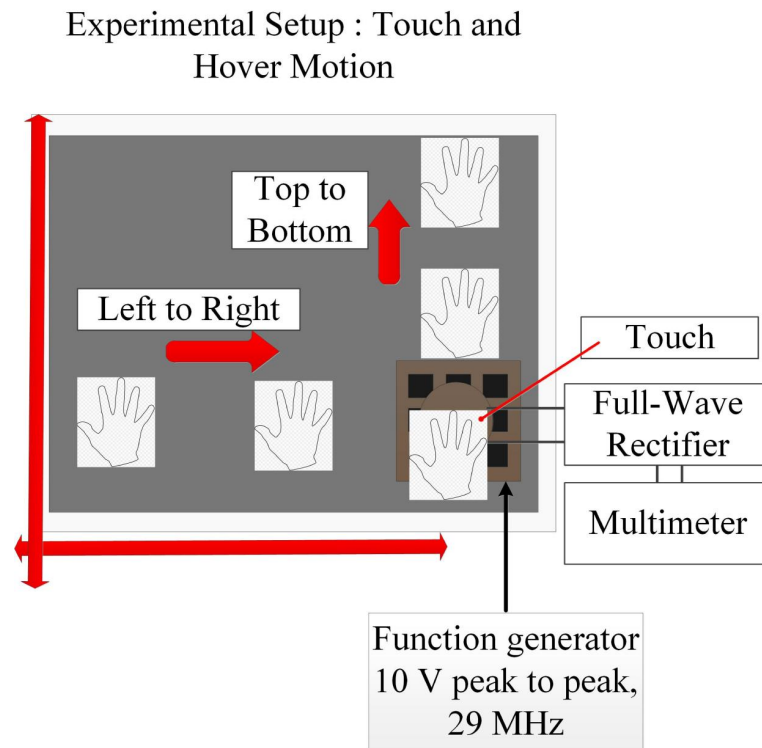
FIGURE 4.19: Experimental setup: touch sensing and hover sensing.

Tx and Rx of the WET sensing system causes a negligible drop of Rx output voltage, resulting in an output value of 3.06V as compared to a previous value of 3.11V as seen in fig.4.24 (a). The LCD used for this test was that of an HP ProBook 4421s. The Laptop display functioned normally. Fig.4.24 (b), demonstrates the test case, where the copper sheet of 150 mm $\times$ 150 mm dimensions was placed on top of the LCD display, which is in turn placed between Tx and Rx. The reduced Output voltage was observed to be 2.94V. This is in-line with our previous finding [14],[15], where the role played by eddy current for wireless power and data transfer through open metal walls was investigated.
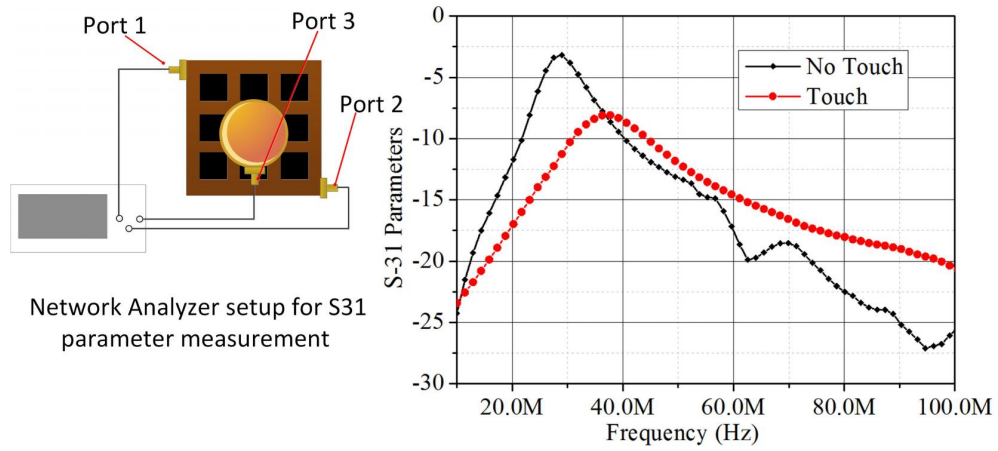
FIGURE 4.20: S-31 parameters for touch and no-touch conditions.
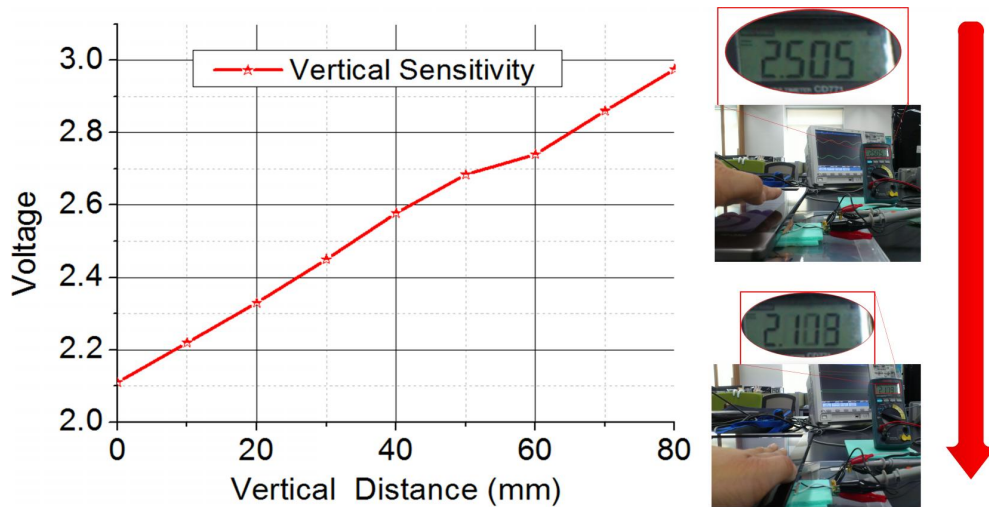


FIGURE 4.21: Voltage (V) vs. Distance (mm) sensitivity: vertical.
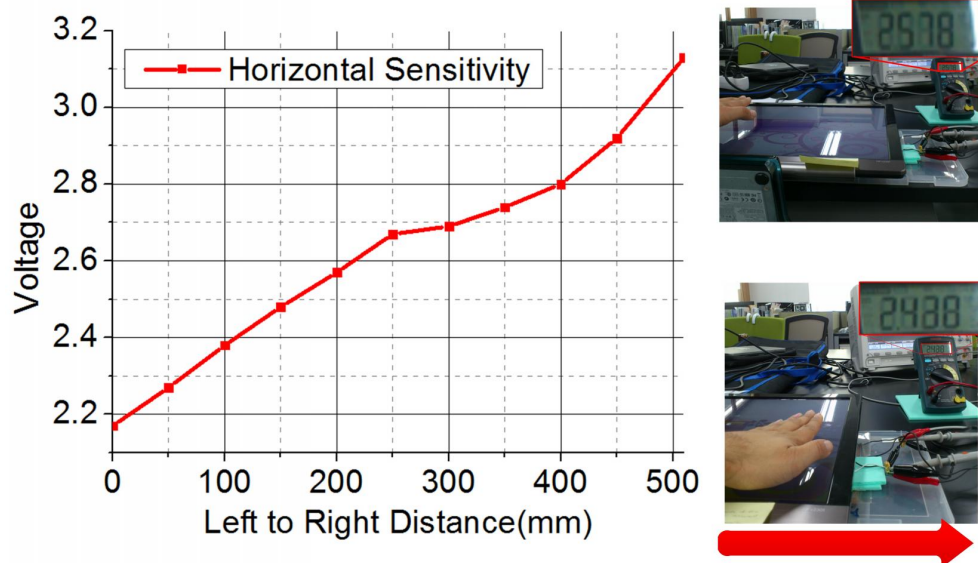
FIGURE 4.22: Voltage (V) vs. Distance (mm) sensitivity: Horizontal.

TABLE 4.1: Summary of voltage changes for various experimental results

| Experiment | Initial voltage (V) | Final voltage (V) | Difference(mV) |
|---|---|---|---|
| **Touch** | **3.27** | **2.11** | **1157** |
| **Hover/Proximity** | | | |
| **Vertical** | **3.16** | **2.29** | **870** |
| **Left-Right** | **3.16** | **2.29** | **870** |
| **Top-Bottom** | **3.16** | **2.3** | **860** |

In either of the test cases except for a small voltage drop, no effects in the display performance have been observed. However, as the proposed WET sensing system presented in this thesis is to be integrated behind the LCD screen, eddy current and EMI effects can be effectively shielded by use of a simple faraday mesh. The other possible methods would be (a) Use of equal TX and Rx physical sizes. (b) Use of radiation suppression techniques [13].
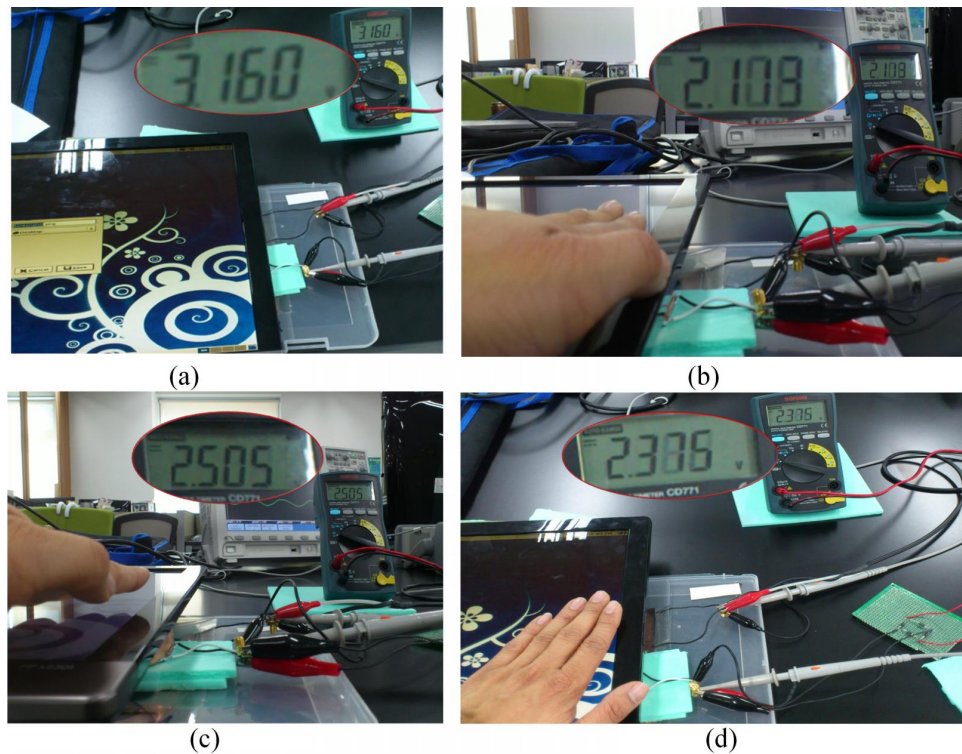
FIGURE 4.23: Sensing demonstration (a) No Touch (b) Touch (c) Proximity (d) Hover motion (top to bottom).

## 4.3.4 Calibration-Effects on Voltage Variations Due to User Hand Sizes

It was necessary to test the differences in the voltage variations due to different sizes of the user hand. This stems from the concern that the magnitude of the voltage drop depends on the area occupied by the user hand over the copper sense head (copper sense head indicated in fig.3.b). To test this, ten volunteers with different hand sizes were asked to perform three simple tasks: touch, proximity and hover motions. No voltage variation between the volunteer with largest hand size to the smallest hand size was observed. For proximity, the voltage variation between largest hand sizes to smallest hand size was 20 mV.i.e. 2.495V for large hand, 2.505 V for medium hand and 2.513V small hand. Likewise hover sensing case, followed pattern of proximity the variations were 19-20 mV. As far as hover and proximity is concerned, that definitely may have some effect of human hand size. But, the variations are very small in the present proposed system. So, a read out IC which not sensitive to such a minute difference can be
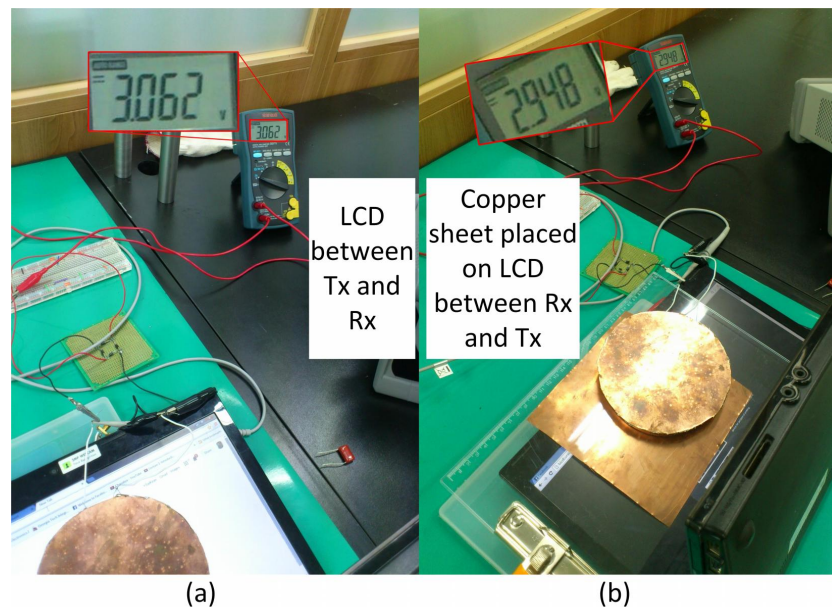
FIGURE 4.24: (a) LCD between Tx and Rx (b) Copper sheet placed atop the LCD between Tx and Rx.

used. There are two solutions to nullify these effects to a great extent: (a) an array of Tx and Rx systems, the size of the Tx and Rx has to be reduced. Which will increase the operation frequency. The operation frequency can be kept low by use of Arlon- 1000 as a dielectric material. However the individual Tx and Rx units have to be shielded from each other to avoid cross unit interference (b) Fuzzy logic based post-processing system, based on the assumption that distance and voltage variation will be different for different sizes of human hands as indicated by the ten volunteer experiment conducted during this research. This would mean calibration is not possible due to imprecision. Hence one is looking at the classic problem of fuzzy logic, where definitions of degrees change according to different users. This can be easily resolved by usage of simple min-max operation circuits, which are low cost and simple to build at a large scale. A similar problem was dealt with, which was related to battery management for electric vehicles using low cost Hybrid-Neuro Fuzzy logic [35].

## 4.4   Summary

### Power and Data

- *Sheet-like waveguide transmitter and cylindrical wave cavity receiver across open metal sheets.* Transmits signal across open metal walls and partially enclosed metal structures. Too weak to transmit power.

- *Sheet-like waveguide transmitter and spiral coil receiver.* Spiral coil receiver is able to receive power across across via metal walls when paired with the sheet-like waveguide

- *Sheet-like waveguide transmitter and spiral coil receiver.* Transmits 280mW watts power upto 400 cm. Transmits 14 watts power upto 120 cm

- *Sheet-like waveguide transmitter and receiver system.* Transmits 16W watts power upto 400 cm. Transmits 40 watts power upto 120 cm. Sustains two way transmission of voice over radio for upto 5 metal complex floors and 300 m within the engine room of the oil-rig

- *Magnetic Flux Manipulation Method.* Successfully transmitted data across perfectly enclosed faraday cage. Using Labview modules across two laptop computers.

### Sensing

- *Hover, Touch and Proximity.* An all in one functionality has been achieved using the proposed system.

- *EMI with other Electronics* There is no evidence of EMI effects when the presented sensor was integrated behind an LCD which was in On-state.

# Chapter 5

# Conclusion

This section draws out the key results and conclusions of the previous chapters. The conclusions have been sectionalized into two parts, the first part deals with the power and data transfer through metal walls, the second part deals with touch, proximity and hover sensing. Both the sections provide an in-depth discussion of the key findings of this work and future applications.

## 5.1 Power and Data Transfer

At the time when this work commenced in late 2013 and early 2014, there were only a few through metal wall wireless power and data transfer systems. Even though, through metal non-invasive systems were present, the problem of limited range, requirement of intermediate systems and perfect alignment had already manifested at the user end. Soon the ship builders realized that a perfect alignment of PUT and EMAT transceivers came with their own constraints[1]-[2]. It is not always possible to ensure alignment, because there is no visibility across metal walls. There were also multi-path induced

fading issues in piezoelectric systems. This work was aimed towards the development of a long range i.e. atleast across two metal rooms without the need of an intermediate system. Free positioning system, by free positioning system it is meant that there is no need for alignment of transceivers.

### 5.1.1 Key Findings

- *SEW at Metal-Air Interfaces in MHz frequency Regime* This is one of the most important point of this work. Until recently, there existed no well established experimental study of SEW's at MHz range at metal-air interfaces. The most recent experimental report was in the range of 0.5 to 20 GHz. The experimental data from the spectrum analyzer indicate towards the existence of SEW's. The theoretical model of Gerson and Nadan [17] was compared with experimental results as shown in 2.5 and 2.6

- *SEW for Power and Data Transfer* This work presents methods to use an important phenomenon to transmit power and data in conditions where through air transmission is not possible. Metal complexes provide EMI shielding to RF waves, the presented method addresses this problem. Although the method has not been studied to address transmission across perfectly enclosed metal chambers. For perfect enclosures, magnetic flux manipulation method could be a way forwards. But it requires a further careful and extensive study.

- *SEW Generation by Intimate Placement of Sheet Like Waveguides Over Metal Surfaces* The interaction of EM waves (which undergo total internal reflection from the metal surfaces) with metal-air interfaces causes a setup of forward and backward surface waves. This work establishes one method to do so, by placing the planar sheet like waveguides intimately to the metal. The generated surface waves can be collected by a receiver which is also placed close/intimately to the metal.

- *Simplified Equivalent Circuit Model* This work presented simplified equivalent circuit models as an effective, practical and alternative method to rigorous EM

solution in order to model and design SEW based wireless systems. These models have been validated by experimental results.

- *SEW Solution and Free Positioning System* Based on the aforementioned key findings, a free positioning wireless power and data transfer system was realized and tested in a real time environment.

### 5.1.2 Antenna and Surface Electromagnetic Wave

The heart of the system presented in this work is the antenna and its capability to generate a surface electromagnetic wave at the metal-air interfaces. The comparison between the PUT, EMAT system with the work presented in this thesis has been summarized in Table 5.1.

TABLE 5.1: Metric comparison with PUT and EMAT solutions

| | Methods | | |
|---|---|---|---|
| | **PUT** | **EMAT** | **This Work** |
| **Type** | Through | Through | Via |
| **Power (W)** | 50 | NA | 40 |
| **Power Transfer Range** | $63.5\ mm$ | $20\ mm$ | 10 to 400 $cm$ |
| **Power Efficiency** $(\%)$ | 51 | 4 | 94 |
| **Frequency Range** $MHz$ | 4 | 1 | 13-25 |
| **Transceiver Coaxial alignment** | Must | Must | Free Position |
| **Communication Range** | $63.5\ mm$ | $20\ mm$ | 300m |
| **Across number of metal floors** | None | None | 5 |
| **Communication system power** $(Watts)$ | NA | 1.23 | 4 |
| **Communication system type** | Digital | Digital | CB Radio, extendable to digital |
| **Real-time testing** | NA | No | **Oil-Rig** |
| **Number of intermediate modules** | atleast 4 | atleast 4 | **None** |

## Advantages

The following points indicated the advantages the presented SEW system has over the state of the art systems.

- *True Electromagnetic System.* The presented system is clearly a true electromagnetic antenna based transceiver system unlike the PUT and EMAT systems which are transducer based systems. This gives the inherent advantage to the presented system, it can transmit data/signal/power to longer distances.

- *Range.* Clearly the presented SEW system, transmits power across 80 mm thick metal wall of ship grade steel. Transmits 16 watts of power across 400 cm, 40 watts upto a range of 1.2 meters, this was one of the objectives of the project. Higher powers can be transmitted, but they have not been pursued further. The radio signal transmission was achieved upto 300 meters within the oil-rig's engine room. A transmission of radio signals upto atleast 5 metal floors was achieved, which surpassed the original transmission across two rooms requirement.

- *Free Positioning System.* Unlike the PUT and EMAT system,the presented SEW system does not require co-axial alignment . This is because the surface waves travel over the metal-air interfaces, while they do so, they carry the power or signal across the metal. These traveling surface waves can be collected by the receivers placed intimately to the metal .

- *Power Transfer Efficiency.* The power transfer efficiency of the proposed system is clearly much higher than the existing systems. If one considers only the efficiency of power transfer across 80 $mm$ thick metal wall, the SEW is clearly superior in performance as compared to PUT and EMAT, it is also evident from the table 5.1.

- *Frequency Range.* The frequency of operation presented in this work was between 13 to 25 $MHz$. It is possible to transmit a data rate of 26 to 50 $Mbps$ binary data.

- *Intermediate Modules.* The presented SEW system does not require intermediate modules to transmit data across two rooms, evident from the range of data transmission capabilities demonstrated by the system.

- *Communication System Type.* A citizen band (CB) radio was installed with the proposed sheet like waveguide transmitter-receiver . Initial feasibility test to migrate towards digital system e.g. WIFI AP were successful.

## 5.2 Wireless Power Transfer Based Sensing System

When this work was undertaken, there were several other kind of touch, proximity and hover sensors were in existence. However, they had constraints of linearity, conductivity of the target object, range. So logically to solve these problems, one of the best solutions was to utilize wireless power transfer systems which transmit power at optimal efficiency at resonance matched condition, in other words impedance matching. (i.) When it touches the receiver or transmitter it changes the impedance on either side (ii.)When a human finger or body comes in proximity and (iii.) When hovers around the transmitter or receiver it offers changes in dielectric constant around the receivers or transmitters. All these three conditions disturbs the resonance condition and hence the change in voltage levels at the receiver can be utilized to register touch, proximity or hovering.

### 5.2.1 Key Findings

- *Wireless Power Transfer and Impedance* Human finger touch on either the receiver or the transmitter of the wireless power transfer system, disturbs the impedance matching condition. This causes a drop in the power transfer efficiency. When

this drop is translated into voltage levels, the voltages drop. This drop in voltages can be utilized to register a touch. This is theoretically mentioned in fig. 2.7 and equation 2.16 and 2.17. Between frequency ranges of 10 to 50 MHz, human hand or finger offers an impedance of 1000 $\Omega$

- *Wireless Power Transfer and dielectric constant* Between 10 to 50 MHz range the human hand or finger dielectric constant is between 100-120. So, whenever a human hand or finger comes in close proximity to the WPT system, it introduces an abrupt change in dielectric constant, which effects the reactance of the transmitter and the receiver.

- *Wireless Power Transfer and EMI with other electronic circuitry* A radiating transmitter of the WPT system will definitely cause EMI to other nearby electronic circuitry. However it can be avoided if one uses a near-field evanescent wave/field based WPT system. The property of the evanescent field is that, the EM fields decompose exponentially in the normal direction to the surface of the transmitter and receiver. Which ranges between 1 to 5 mm. Beyond 5 mm there is no power transmission of any kind.

- *WPT Sensor, Sheet-Like Waveguide and Evanescent Fields* In this work, the sheet-like waveguide WPT systems were used for their inherent advantages. They offer evanescent fields which decompose exponentially normal to their surface. Apart from this since a sheet like waveguide has a dominant surface reactance, it effects the power transfer efficiency. Henceforth, as evident from the equation 2.19 to 2.23 the factors like sheet reactance and dielectric constant play a dominant role in deciding the power transfer efficiency. Hence, an all in one touch, proximity and hover sensor is realized. At the same time this sensor does not cause EMI to the nearby circuitry.

## Advantages

- *All in one Touch, Proximity and Hover Sensing.* The presented WPT sensor plays the triple role of touch, proximity and hover sensing, which is unique.

- *Planar.* Being planar in geometry, they do not require additional space allotment within the TSP's.

- *Easy to Integrate.* Because they can operate even when placed behind the LCD screens under "ON" mode. Also, they do not show any effect on neither the LCD performance, nor their own performance. The proposed system can be easily integrated behind the ordinary LCD's and convert them into TSP's. This eliminates the need of special fabrication techniques.

- *Sensitivity, Linearity and Range.* Being electromagnetic in nature they show linear performance over large range. sensitivity vs range characteristics as seen in fig 4.21 and 4.22.

- *No RC Time constant Delays for Large or Contoured Displays* Since the operation principle is not capacitive or resistive in nature, the system has all the advantages of inductive touch sensing. However, unlike inductive TSP , the proposed sensor does not require a stylus.

# Additional Applications

*Metal Detection System.* Based on the first part of power/electronic signal transmission over the metal surfaces, the same system can be utilized to conduct metal sensing or metal detection system.

*Metal Length Determination.* It is also worth noting that the presented system is never electrically in contact with the metal. Hence it is possible to utilize the same system to measure the length of a moving metal structure based on the transmitted and received signal strengths. e.g. iron and steel Billets, blooms, rail mill-shops.

# Chapter 6

# Supporting Information

## Supporting video links

### Power Transfer Demo 400 cm

https://www.youtube.com/watch?v=rq-_2od7gW0

### Power Transfer Demo 40 Watts and safety test

https://www.youtube.com/watch?v=6mEhi9OFI3w

### Communication Demo (Sai's Cam)

https://www.youtube.com/watch?v=iSm66fGOs2I

### Communication Demo( Quang's Cam extended)

https://www.youtube.com/watch?v=iONoNp2RMqU

## 280 mW detailed demo

https://www.youtube.com/watch?v=tdnM_V2Ywoc

# Bibliography

[1] Lawry, T.J., Saulnier, G.J., Ashdown, J.D., Wilt, K.R., Scarton, H.A., Pascarelle, S. and Pinezich, J.D., "Penetration-free system for transmission of data and power through solid metal barriers," MILITARY COMMUNICATIONS CONFERENCE, vol., no., pp.389-395, 7-10 Nov. 2011

[2] Graham, D.J., Neasham, J.A. and Sharif, B.S., "Investigation of Methods for Data Communication and Power Delivery Through Metals," IEEE Transactions on Industrial Electronics, vol.58, no.10, pp.4972-4980, Oct. 2011

[3] Oruganti, S.K., Heo, S.H., Ma, H., Bien, F. "Wireless energy transfer-based transceiver systems for power and/or high-data rate transmission through thick metal walls using sheet-like waveguides," Electronics Letters , Vol.50, no.12, pp.886-888, June 5 2014

[4] Oruganti, S.K., Bien, F. "Investigation of near-field wireless energy transfer for through metal-wall applications," IEEE WPTC-2014, Jeju- Korea, pp.247-250, 8-9 May 2014

[5] C. Hong, L. Chu, W. Lai, A.-S. Chiang, and W. Fang, ?Implementation of a new capacitive touch sensor using the nanoporous anodic aluminum oxide (np-AAO) structure, IEEE Sensors Journal, vol. 11, no. 12, pp. 3409-3416, Dec. 2011.

[6] W. H. Ko and W. Qiang, "Touch mode capacitive pressure sensors," Sens. Actuators A, Phys., vol. 75, no. 3, pp. 242-251, 1999.

[7] E. So, H. Zhang, and Y.-S. Guan, "Sensing contact with analog resistive technology," in Proc. IEEE Int. Conf. Syst., Man, Cybern. IEEE SMC, vol. 2, pp. 806-811, Oct. 12?15, 1999.

[8] G. Barrett and O. Ryomei, "Projected-capacitive touch technology," Inf. Display, vol. 26, no. 3, pp. 16?21, 2010.

[9] S. Lee and S. Zhai,"The performance of touch screen soft buttons," in Proc. SIGCHI Conf. Human Factors Comput. Syst., pp. 309-318, 2009.

[10] L. Stark "Electromagnetic waves in periodic structures" Technical report No. 208, Dec 1952.

[11] Vander Voot, G.F., "Metallography, Principles and Practice" Mcgraw-Hill College,pp 442,1984.

[12] Sommerfeld, A. "*ü*ber die Ausbreitung der Wellen in der drahtlosen Telegraphie", Annalen der Physik Vol. 333, no. 4, pp 665-(36), 1909

[13] Polo, J.A., Lakhtakia, A. "Surface electromagnetic waves- A review." Las. and Phot. Rev. Vol. 5, no. 2, pp 234-246, 2011

[14] Baíbakov, V. I., Datsko, V.N., Kistovich, Y,V. "Experimental discovery of Zennecks surface electromagnetic waves." Sov. Phys. Usp. Vol.32, no. 4, pp 378-379, 1989

[15] Datsko, V.N. "On surface electromagnetic waves." Journal of Comm. Tech. and Elec., Springer, 59, no. 5, pp 414-418, 2014

[16] Maier, S.A., "Plasmonics: Fundamentals and Applications." Springer., pp 21-37, 2007

[17] Gerson, T.J., Nadan, J.S. "Surface Electromagnetic Modes of a Ferrite Slab," Microwave Theory and Techniques, IEEE Transactions on ,vol. 22, no.8, pp.757-763, Aug 1974

[18] Oruganti, S.K., Bien, F. "Flexible wireless energy transfer systems by carbon fiber as a dielectric material: Study and experiments," IEEE WPTC-2013, Perugia Italy , pp.159-162, 15-16 May 2013

[19] Noda, A., Shinoda, H. "Selective Wireless Power Transmission Through High- Q Flat Waveguide-Ring Resonator on 2-D Waveguide Sheet," IEEE Transactions on Microwave Theory and Techniques, vol.59, no.8, pp.2158-2167, Aug. 2011

[20] S. G. Lee, H. Hoang, Y. H. Choi, and F. Bien, "Efficiency improvement for magnetic resonance based wireless power transfer with axialmisalignment," Electron. Lett., vol. 48, no. 6, pp. 339-340, Mar. 2012.

[21] H. Hoang, S. Lee, Y. Kim, Y. Choi, and F. Bien, "An adaptive technique to improve wireless power transfer for consumer electronics," IEEE Trans. Consum. Electron., vol. 58, no. 2, pp. 327-332, May 2012.

[22] J. Huh, S. Lee, C. Park, G.-H. Cho, and C.-T. Rim, "High performance inductive power transfer system with narrow rail width for on-line electric vehicles," in Proc. IEEE Energy Convers. Congr. Expo. (ECCE), Sep. 2010, pp. 647-651.

[23] Oruganti, S.K., Sang Hyun Heo, Hyunggun Ma, Bien, F. "Wireless Energy Transfer: Touch/Proximity/Hover Sensing for Large Contoured Displays and Industrial Applications," IEEE Sensors Journal, vol.15, no.4, pp.2062-2068, April 2015

[24] Noda, A., Shinoda, H. "Selective proximity power transmission using low leakage ribbon waveguide and high-Q resonant coupler," SICE Annual Conference (SICE), 2011 Proceedings of , vol., no., pp.836-841, 13-18 Sept. 2011

[25] Noda, A., Shinoda, H. "The lower-bound of electromagnetic leakage of 2D wireless power transmission," Networked Sensing Systems (INSS), 2010 Seventh International Conference on , vol., no., pp.138-144, 15-18 June 2010

[26] H. Kanai, I. Chatterjee, and O. P. Gandhi, "Human body impedance for electromagnetic hazard analysis in the VLF to MF band," IEEE Trans. Microw. Theory Techn., vol. 32, no. 8, pp. 763-772, Aug. 1984.

[27] B. Sanchez, A. L. P. Aroul, E. Bartolome, K. Soundarapandian, and R. Bragos, "Propagation of measurement errors through body composition equations for body impedance analysis," IEEE Trans. Instrum. Meas., vol. 63, no. 6, pp. 1535-1544, Jun. 2014.

[28] F. Ruan, T. Dlugosz, D. Shi, and Y. Gao, "Cylinder model of human body impedance based on proximity effect," in Proc. 3rd IEEE Int. Symp. Microw., Antenna, Propag. EMC Technol. Wireless Commun., Oct. 2009, pp. 16-19.

[29] V. De Santis, P. A. Beeckman, D. A. Lampasi, and M. Feliziani, "Assessment of human body impedance for safety requirements against contact currents for frequencies up to 110 MHz," IEEE Trans. Biomed. Eng., vol. 58, no. 2, pp. 390?396, Feb. 2011.

[30] C. Gabriel, S. Gabriel, and E. Corthout, "The dielectric properties of biological tissues: I. Literature survey," Phys. Med. Biol., vol. 41, no. 11, pp. 2231-2249, 1996.

[31] S. Gabriel, R. W. Lau, and C. Gabriel, "The dielectric properties of biological tissues: II. Measurements in the frequency range 10 Hz to 20 GHz," Phys. Med. Biol., vol. 41, no. 11, pp. 2251-2269, 1996.

[32] Y. Makino, K. Minamizawa, and H. Shinoda, "Two dimensional communication technology for networked sensing system," in Proc. Int. Workshop Netw. Sensing Syst. (INSS), pp. 168-173,2005.

[33] C. J. Chen, T. H. Chu, C. L. Lin, and Z. C. Jou, "A study of loosely coupled coils for wireless power transfer," IEEE Trans. Circuits Syst. II, Exp. Briefs, vol. 57, no. 7, pp. 536-540, Jul. 2010.

[34] J. Lee and S. Nam, "Fundamental aspects of near-field coupling small antennas for wireless power transfer," IEEE Trans. Antennas Propag., vol. 58, no. 11, pp. 3442-3449, Nov. 2010.

[35] F. Zhang, X. Liu, S. A. Hackworth, R. J. Sclabassi, and S. Mingui, "In vitro and in vivo studies on wireless powering of medical sensors and implantable devices," in Proc. IEEE/NIH Life Sci. Syst. Appl. Workshop (LiSSA), Apr. 2009, pp. 84-87.

[36] Smith, G.S., Petersson, L.E.R. "On the use of evanescent electromagnetic waves in the detection and identification of objects buried in lossy soil," IEEE Transactions on, Antennas and Propagation,vol.48, no.9, pp.1295-1300, Sep 2000

[37] Mikki, S.M., Antar, Y.M.M. "A Theory of Antenna Electromagnetic Near Field-Part II," IEEE Transactions on Antennas and Propagation, vol.59, no.12, pp.4706-4724, Dec. 2011

[38] Compton, R.C., Rutledge, D.B., "Approximation Techniques for Planar Periodic Structures," IEEE Transactions on Microwave Theory and Techniques, vol.33, no.10, pp.1083-1088, Oct 1985

[39] C.W. Van Neste, J.E. Hawk, Arindam Phani, J.A.J. Backs, Richard Hull, Tinu Abraham, S.J. Glassford, A.K. Pickering and Thomas Thundat . "Single-contact transmission for the quasi-wireless delivery of power over large surfaces. Wireless Power Transfer", 1, pp 75-82, 2014. doi:10.1017/wpt.2014.9